Title
A CLUSTER MULTIPLE-SCATTERING THEORY FOR MEDIUM ENERGY ELECTRON DIFFRACTION

Authors
Barton, J.J.
Xu, M.L.
Van-Hove, M.A.

Publication Date
1988

LBL-23212
Preprint

Lawrence Berkeley Laboratory
UNIVERSITY OF CALIFORNIA

Materials & Chemical Sciences Division

Submitted to Physical Review B

A Cluster Multiple-Scattering Theory for Medium Energy Electron Diffraction

J.J. Barton, M.-L. Xu, and M.A. Van Hove

January 1988

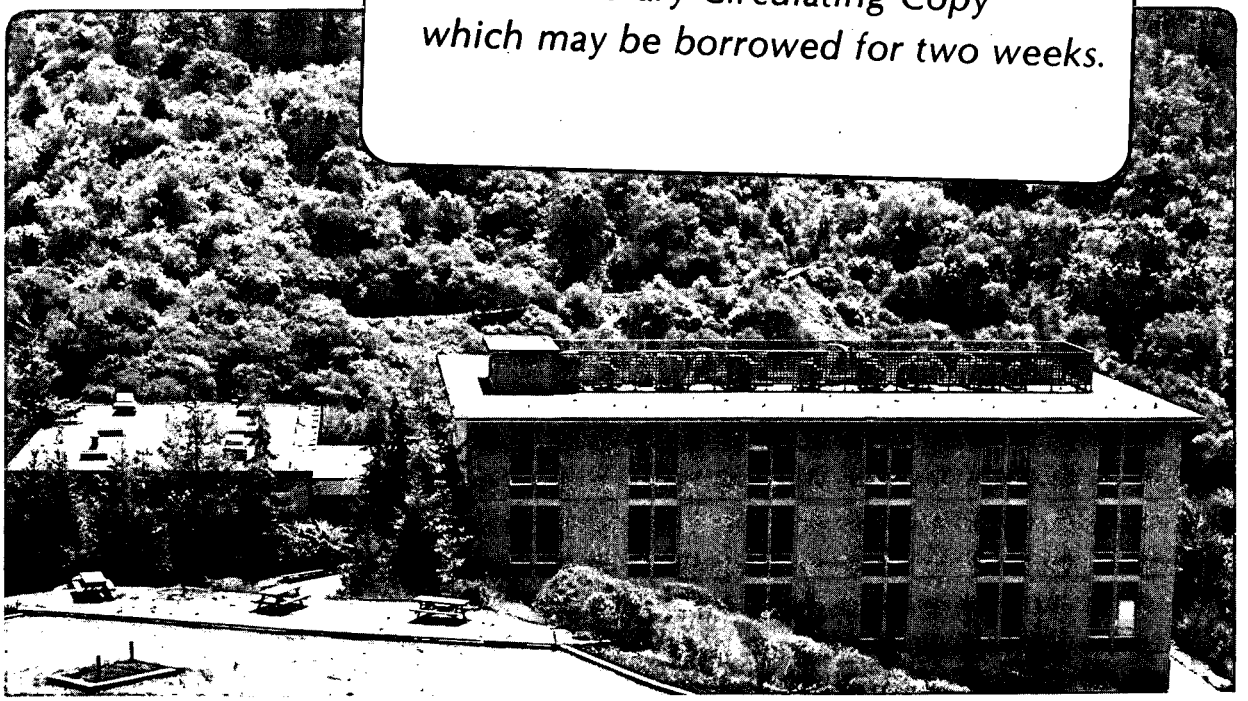

Prepared for the U.S. Department of Energy under Contract DE-AC03-76SF00098

DISCLAIMER

LBL-23212

A Cluster Multiple-Scattering Theory for Medium Energy Electron Diffraction

J.J. Barton* , M.-L. Xu, and M. A. Van Hove

Materials and Chemical Sciences Division

Lawrence Berkeley Laboratory, Berkeley, CA 94720

Submitted to Physical Review B on January 9, 1988

Abstract

A theory of Medium Energy (100–5000eV) Electron Diffraction (MEED) is developed from a multiple-scattering curved-wave theory of photoelectron diffraction. It may be called "Near-Field Expansion in Clusters". Only selected important scattering events are included and these are computed in times proportional to electron wave number by using a generalized scattering factor method (conventional LEED methods require computations proportional to at least the fourth power of the wave number, while the "chain" method for MEED scales as at least the square of the wave number). This removes the most serious barrier to a multiple-scattering analysis for surface structure determination. A direct summation over atoms and scattering

paths is used, avoiding any assumptions of periodicity in the surface structure. The theory allows a clearer understanding of the relationship between diffraction intensities and surface structure than heretofore possible.

PACS numbers: 61.14.Dc,61.14.Hg,61.55.Fe

I. INTRODUCTION

Recent efforts[1] to determine surface structures with photoelectron diffraction in the form of angle-resolved photoemission extended fine structure (ARPEFS) have led to considerable advances in the understanding of electron scattering in the intermediate energy (100–1000 eV) range. Three developments are particularly important. First, by studying the nature of atomic scattering factors, Orders and Fadley[2] were able to reconcile the observed sensitivity of normal emission photoelectron diffraction to interplanar spacing with the localized cluster model for photoelectron diffraction of Lee.[3] Second, new experimental measurements demonstrated that only a small number of atoms near the photoemitter contribute significant signal to the ARPEFS curves.[4] And, third, a new method of calculating curved-wavefront multiple-scattering wavefunctions, applicable to the intermediate energy range has been derived.[5] This last development is vital since multiple forward scattering is known to be large in this energy range,[6] and since curved-wavefront corrections must be included for forward scattering,[7] precluding quantitative analysis with plane-wave single-scattering theory.

In this paper we apply the new insight and new multiple-scattering for-

mulas developed for ARPEFS to the problem of simulating medium energy electron diffraction (MEED). By "medium" energies we mean roughly 100-5000eV. Our upper limit is determined only by our treatment of elastic scattering as potential scattering. At some high energy, our spherical wave scattering factors will converge to the Born approximation of plane wave scattering factors. Thus, in principle our theory should apply even into the energy range (10-40keV) of reflection high energy electron diffraction. However, we have not yet explored the energy range beyond 1000eV, preferring instead to concentrate on the more demanding range between 100 and 1000eV.

Among the advantages to working at electron energies above those of Low Energy Electron Diffraction (LEED) we emphasize one in particular: The angular distribution for electron scattering from ion-cores in this energy range becomes increasingly anisotropic with a pronounced forward peak. We will exploit this anisotropy in multiple-scattering calculations to reduce the number of scattering events considered and hence the computational effort. With experience, this forward peaking may also be useful in selecting experimental geometries that maximize sensitivity to particular structural features.[8]

To take advantage of the scattering anisotropy, we shall abandon the methods which have been devised for self-consistent, full-order multiple-scattering in the LEED energy range[9,10,11] in favor of a simple, iterative cluster method. As described in Section II, an important by-product of this cluster method is a very direct connection to ARPEFS theory, allowing much of the experience gained in the study of photoelectron diffraction to

be applied to the MEED problem. Furthermore, as recent work in LEED theory demonstrates,[12] cluster-type theories may be advantageous for large-unit-cell structures and for disordered surfaces.

Other theories exist for MEED and RHEED. The quasi-dynamical method,[13] also used in LEED, simply ignores multiple-scattering within individual layers and uses a LEED layer stacking scheme in a plane-wave representation. The computation time of this method depends upon the number of beams retained between layers and it is particularly successful for systems with large interlayer spacings. Unfortunately, the neglect of intralayer scattering is not always justified, especially for grazing angles of electron incidence. The "chain" method developed by Pendry, Gard, and Masud[14] exploits the predominance of forward scattering in the medium energy range by first solving the multiple-scattering in isolated chains of atoms, followed by a merging of the chains into layers and of layers into a crystal. The intra-chain multiple-scattering computations are proportional to at least $l_{\max}$ squared, where $l_{\max}$ is the largest angular momentum included. This is a marked improvement over the intra-layer computations of LEED theories, which require at least the fourth power of $l_{\max}$. Thus the useful energy range can be extended up to about 5000eV. (We explore application of the present method to chains in Ref. 8.) Maksym and Beeby[15] start from the high-energy limit with a RHEED theory based upon a plane-wave expansion of the atomic scattering and on a 2-D plane-wave representation coupled with numerical integration perpendicular to the surface. They have extended[16] the method to MEED energies in the range 5-10keV by applying a LEED layer stacking method.

We shall describe in Sec. II the conceptual framework we will use to discuss the multiple-scattering problem and to connect it to the ARPEFS theory. Sec. III develops the multiple-scattering equations for an incident plane wave using the TS-MQNE elastic scattering method. Qualitative analysis of MEED intensities in terms of interference path length differences is covered in Sec. IV. Sec. V begins the discussion of applications of our methods by investigating the numerical convergence of the multiple-scattering formulas, while Sec. VI discusses the qualitative analysis of the MEED specular reflection from Ni(001). In Sec. VII we give a brief comparison to other appoaches to MEED intensities.

II. CLUSTER EXPANSION TREE

The cluster expansion multiple-scattering method is a perturbation method which assumes that the complete scattered electron wavefunction can be written in terms of a finite number of individual scattering events. We write the total wavefunction Ψ as a series beginning with the incident plane wave, $e^{i\mathbf{k}_{in}\cdot\mathbf{a}}$, normalized to unit current per unit area normal to $\mathbf{k}_{in}$.

We organize the calculation of the scattered wave into "trees" representing scattering paths connecting the scattering ion-cores, cf. Fig. 1. There is one tree for every atom in the surface. We call the first atom in a given tree the "trunk" atom of its tree. Branches of a particular tree connect a given atom with every atom near enough and in a favorable enough position to receive significant flux from it.

Observe that, except at the trunk atom, the tree scattering for MEED is the same as the tree scattering for angle-resolved photoemission extended

fine structure (ARPEFS). The main goal of this paper is to apply the new theory of ARPEFS in Ref. 17 to MEED.

ARPEFS results from photoelectron diffraction: the interference between alternative paths open to a photoelectron as the result of numerous elastic scattering collisions. The fine structure consists[4] of oscillations in the form of a cosine series:

$$\chi_{\mathrm{ARPEFS}} = \sum_j A_j \cos(kp_j + \phi_j) \tag{1}$$

where the index j runs over pairs of scattering paths. Here A_j is the product of the amplitude of two interference paths, ϕ_j is the difference in scattering potential phase shifts for the two paths, and p_j is the difference in the length of the paths. The path length difference for all pairs of paths can be written as

$$p_j = \sum_i (a_i - \mathbf{a}_i \cdot \hat{\mathbf{R}}) = \sum_i a_i(1 - \cos\theta_{\mathbf{aR}}) \tag{2}$$

where the vectors $\mathbf{a}_i$ are bond vectors between two atoms in the surface and $\mathbf{R}$ points into the detector.

For ARPEFS, the trunk atom has been photoexcited to give an angular distribution of electron amplitude determined by the photoemission matrix element. For MEED, the trunk atom has been "excited" by the incident plane wave to give an elastically scattered spherical wave whose angular distribution is governed by atomic scattering factors. The remainder of the tree is formed under the same conditions in ARPEFS and in MEED with ARPEFS single-scattering corresponding to MEED double-scattering and so on. To complete the ARPEFS problem we square the tree scattering amplitude and then sum over the photoexcited trunk atoms. To complete

the MEED problem, we must form trees for all atoms reached by the incident plane wave, sum their amplitudes and square to calculate the intensity.

Thus our understanding of the physics of the ARPEFS scattering can be transfered to study the multiple-scattering part of the the MEED problem:

i)we expect some of the MEED oscillations to have the form $\cos[ka_i(1-\cos\theta_{\mathbf{aR}})+\phi_i]$, where k is the electron wave number, $|\mathrm{a}_i| = a_i$ is the length of some branch of a tree, $\theta_{\mathbf{aR}}$ is the angle between the branch and the direction of the detector (MEED spot), and ϕ_i is an ion-core potential phase shift;

ii)the largest part of the scattered wave amplitude should come from primary branches connecting the trunk atom to nearest neighbor atoms and to backscattering atoms in the shells further from the trunk atom;

iii)the only significant secondary and higher branches will include forward-scattering events at all or most of the higher order branch-points; and

iv)curved wavefront corrections will be required in MEED formulas as in the ARPEFS formulas.[7] We shall include them here via the Taylor Series Magnetic Quantum Number Expansion Method (TS-MQNE).[5]

We can also expect to find important differences between the ARPEFS and MEED problems. The coherent illumination of the surface by the incident electron beam results in many more interference pairs than are possible in ARPEFS. In the next section we develop our multiple-scattering equations for MEED from the ARPEFS model so that we can explore a path length difference analysis for MEED.

III. TAYLOR SERIES, MAGNETIC QUANTUM NUMBER EXPANSION FOR AN INCIDENT PLANE WAVE.

In this section we give the formulas for the scattered wave emanating from each branch point (atom) in one cluster tree, tracing through a connected, arbitrary set of branches. In the next section we shall sum over all the branch points and discuss the resulting interference.

We label the trunk atom by **0**, the vector from the coordinate origin to the trunk atom. Thus a single-scattered wave $\psi_{\mathbf{0}}(\mathbf{r})$ emanates from **0**. The vector **a** runs between the trunk atom and second-scattering atom, along a primary branch of the tree; similarly **b** connects second and third scattering atoms. Note that these vectors are "bond" vectors: the coordinates of the triple-scattering atom are given by $\mathbf{0}+\mathbf{a}+\mathbf{b}$. The scattered wavelets will be subscripted by the vectors defining the path of the electron, e.g. $\psi_{\mathbf{0ab}}$.

We adopt the coordinate axes of Ref. 7, appendix B: the scattering angle between **a** and **b** will be written $\theta_{\mathbf{ab}}$ and the dihedral angle between the plane containing the vectors **0** and **a** and the plane containing the vectors **a** and **b** will be $\phi_{\mathbf{0ab}}$. To aid in building up to the multiple-scattering case we shall use spherical harmonics from the outset, rather than the simpler Legendre polynomials. This requires us to introduce a reference axis **x** which we might select in the plane of the surface. It will not appear in the final formulae.

We will build directly upon the results of Ref. 7. A plane wave with propagation vector $\mathbf{k}_{in}$ scatters from the trunk atom, which we assume to be represented by a spherically symmetrical muffin-tin potential, to give

$$\psi_{\mathbf{0}}(\mathbf{r}) = e^{i\mathbf{k}_{in}\cdot\mathbf{0}}\sum_{l=0}^{l_{max}}\sum_{m=-l}^{l} T_l(k)4\pi i^l h_l(kr')Y_{lm}(\hat{\mathbf{r}}')Y^*_{lm}(\hat{\mathbf{k}}_{in}).$$

Here we use $\mathbf{r} = \mathbf{0} + \mathbf{r}'$,

$$T_l(k) = \frac{1}{2}(e^{i2\delta_l(k)} - 1)$$

for partial wave phase shifts $\delta_l(k)$, spherical Hankel functions (outgoing spherical waves) h_l, and spherical harmonics Y_{lm}. The factor $e^{i\mathbf{k}_{in}\cdot\mathbf{0}}$ gives the phase of the incident wave at the center of the scattering potential. This equation is valid anywhere outside the muffin-tin radius.

At our detector (e. g. LEED screen), at position $\mathbf{r}' = \mathbf{R}$, we can replace $h_l(kr')$ by its asymptotic form:

$$\begin{aligned} i^l h_l(k|\mathbf{R}-\mathbf{0}|) &\sim \frac{e^{ik|\mathbf{R}-\mathbf{0}|}}{ik|\mathbf{R}-\mathbf{0}|} \qquad k|\mathbf{R}-\mathbf{0}| \gg l(l+1) \\ &\sim \frac{e^{ikR}}{ikR} e^{-ik\hat{\mathbf{R}}\cdot\mathbf{0}} \qquad |\mathbf{R}| \gg |\mathbf{0}| \end{aligned} \tag{3}$$

and recall the scattering amplitude for atomic potentials:

$$f(\theta_{\mathbf{kR}}, k) = \frac{1}{ik}\sum_{l=0}^{l_{max}}\sum_{m=-l}^{l} T_l(k) 4\pi Y_{lm}(\hat{\mathbf{R}}) Y_{lm}(\hat{\mathbf{k}}_{in})$$

to write

$$\psi_0(\mathbf{R}) = e^{i\mathbf{k}_{in}\cdot\mathbf{0}} f(\theta_{\mathbf{k}_{in}\mathbf{R}}) \frac{e^{ikR}}{R} e^{-ik\mathbf{0}\cdot\hat{\mathbf{R}}}.$$

This is the familiar form for the scattered wave from a central potential. The distance $|\mathbf{R}-\mathbf{0}|$ has been expanded as $R - \hat{\mathbf{R}}\cdot\mathbf{0}$. This completes the single-scattering problem: once the partial wave phase shifts are known, the scattered wave can be calculated.

For a double-scattering event, the second atom is likely to be too close for the asymptotic condition, Eq. 3, to apply. Therefore we must consider the wave incident upon the second potential to be a series of spherical waves, $i^l h_l(kr')Y_{lm}(\hat{\mathbf{r}}')$. The contribution at the detector of one of these partial

waves to the wave double-scattered by atoms **0** and **a** may be written with the aid of Eq. (39) in Ref. 5 as

$$\psi_{\mathbf{0a}}^{lm}(\mathbf{R}) = \sum_{m'=-l}^{l} N_{lm'} R_{m'm}^{(l)}(0, \theta_{\mathbf{k}_{in}\mathbf{a}}, \pi - \phi_{\mathbf{x}\mathbf{k}_{in}\mathbf{a}}) \times \sum_{p'=0}^{l-|m'|} c_{p'm'}^{l} e^{im'\phi_{\mathbf{0aR}}} \frac{e^{ika}}{a} \frac{e^{ik|\mathbf{R}-\mathbf{0}-\mathbf{a}|}}{ik|\mathbf{R}-\mathbf{0}-\mathbf{a}|} F_{p'm'}^{00}(k, \mathbf{a}, \hat{\mathbf{R}})$$

where N_{lm} is the normalizing coefficient for spherical harmonics, $R_{m'm}^{(l)}$ is a rotation matrix element taking our coordinate system from $\hat{\mathbf{z}}||\mathbf{k}_{in}$ to $\hat{\mathbf{z}}||\mathbf{a}$, and $c_{p'm'}^{l}$ is a Taylor series coefficient, all defined in Ref. 5. The function $F_{p'm'}^{pm}(k, \mathbf{a}, \hat{\mathbf{R}})$ is a curved wave scattering factor, a generalization of the plane wave scattering amplitude $f(\theta_{\mathbf{aR}})$. This scattering factor takes spherical wave components (p, m) at a source point, translates them a distance $|\mathbf{a}|$ along $\mathbf{a}$, scatters them from the potential at $\mathbf{a}$, and gives the amplitude of scattered spherical wave components $(p'm')$ into a direction $\hat{\mathbf{R}}$.

Our double scattered wave equation is exact, but both the sum on m' and on p' converge rapidly, so we may take their limits to be $m' = \pm\tau$ and $p' = \tau - |m'|$ for τ small. This approximation corresponds[18] to truncating the Taylor series expansion of the angular part of the Fourier transform of $i^l h_l(kr) Y_{lm}(\hat{\mathbf{r}})$ about $\mathbf{r} = \mathbf{a}$. The truncation of the sum on m' may also be viewed as ignoring high magnetic sublevels which cannot overlap the scattering potential. In this view, the purpose of the rotation matrix is to align the scattering axis and the magnetic quantization axis. Then only sublevels which peak near the scattering axis are required. We refer to the truncation of these sums as the Taylor Series, Magnetic Quantum Number Expansion (TS-MQNE).

To give the complete amplitude for double scattering from **0** and then **a**,

we must weight each partial wave by $T_l(k)4\pi Y^*_{lm}(\mathbf{k}_{in})$ and sum over partial waves:

$$\psi_{0\mathbf{a}}(\mathbf{R}) = \frac{e^{ika}}{a}\frac{e^{ik|\mathbf{R}-\mathbf{0}-\mathbf{a}|}}{ik|\mathbf{R}-\mathbf{0}-\mathbf{a}|}e^{i\mathbf{k}_{in}\cdot\mathbf{0}}\sum_{m'=-\tau}^{\tau}\sum_{p'=0}^{\tau-|m'|}\left\{e^{im'\phi_{\mathbf{kaR}}}F^{00}_{p'm'}(k,\mathbf{a},\hat{\mathbf{R}})\right.$$
$$\left.\left[\sum_{l=0}^{l_{max}}\sum_{m=-l}^{l}T_l(k)4\pi Y^*_{lm}(\mathbf{k}_{in})N_{lm}R^{(l)}_{m'm}(0,\theta_{\mathbf{k}_{in}\mathbf{a}},\pi-\phi_{\mathbf{xk}_{in}\mathbf{a}})c^l_{p'm'}\right]\right\}$$

The sums on l and m have been exchanged with the sums on m' and p'. Now the sum on partial waves can be recognized as a special case of the curved wave scattering factor, $F^{p'm'}_{pm}(k,\mathbf{a},\mathbf{b})$ with $p = m = 0$. To further simplify the appearance of the wavefunction we assemble the curved wave scattering factors into scattering matrices:

$$[\mathbf{F}_{\mathbf{a}\hat{\mathbf{b}}}]^{p'm'}_{pm} = (-1)^{|m|+|m'|-|m-m'|/2}F^{p'm'}_{pm}(k,\mathbf{a},\hat{\mathbf{b}}),$$

with a column vector for the case $p' = m' = 0$:

$$[\mathbf{f}_{\mathbf{a}\hat{\mathbf{R}}}]_{pm} = F^{00}_{pm}(k,\mathbf{a},\hat{\mathbf{R}}),$$

and a row vector for $p = m = 0$:

$$\left[\mathbf{f}^T_{\mathbf{k}_{in}\hat{\mathbf{a}}}\right]_{p'm'} = F^{p'm'}_{00}(k,\mathbf{k}_{in},\hat{\mathbf{a}}).$$

Finally, a diagonal matrix is defined to include the magnetic quantum number portion of the rotation matrix:

$$[\mathbf{\Phi}_{\mathbf{k}_{in}\mathbf{ab}}]^{p'm'}_{pm} = \delta_{p'p}\delta_{m'm}e^{im\phi_{\mathbf{k}_{in}\mathbf{ab}}}.$$

The indices are understood to obey $\tau \le m \le \tau'$ and $0 \le p \le \tau - |m|$. Then the double scattered wave becomes

$$\psi_{0\mathbf{a}}(\hat{\mathbf{R}}) = \frac{e^{ikR}}{R}e^{i\mathbf{k}_{in}\cdot\mathbf{0}-ik\hat{\mathbf{R}}\cdot\mathbf{0}}\frac{e^{ika-ik\hat{\mathbf{R}}\cdot\mathbf{a}}}{a}\mathbf{f}^T_{\mathbf{k}_{in}\hat{\mathbf{a}}}\mathbf{\Phi}_{\mathbf{k}_{in}\mathbf{a}\hat{\mathbf{R}}}\mathbf{f}_{\mathbf{a}\hat{\mathbf{R}}}.$$

Once this notation is understood, higher order waves can be written by inspection. For example, the double-scattered wavefunction can be read as three phase and three amplitude terms as follows. The first phase term contains the phase and radial decay common to all of the scattered waves. It contributes nothing significant to our interference observations. The next term is characteristic of plane wave scattering. It gives the phase of the incident plane wave at the trunk atom minus the phase of the outgoing plane wave at the trunk atom. The presence of this term gives rise to the Bragg-like peaks in MEED. The third term is the extra phase and radial decay due to the second scattering event. The three amplitude terms may be read as follows. The wave traveling in the direction $\mathbf{k}_{in}$ scatters into the direction $\hat{\mathbf{a}}$ with amplitude $\mathbf{f}^T_{\mathbf{k}_{in}\hat{\mathbf{a}}}$. The magnetic quantum numbers are rotated about $\mathbf{a}$ from $\mathbf{k}_{in}$ to $\hat{\mathbf{R}}$ by $\mathbf{\Phi}_{\mathbf{k}_{in}\mathbf{a}\hat{\mathbf{R}}}$. Finally, the wave is translated along $\mathbf{a}$, scatters, and exits in the direction $\hat{\mathbf{R}}$ with amplitude $\mathbf{f}_{\mathbf{a}\hat{\mathbf{R}}}$. We have purposefully separated the phase terms from the amplitude terms to aid our path-length difference analysis.

To create formulas for higher order terms we must insert one additional phase term, one $\mathbf{\Phi}$ matrix, and one scattering matrix for each order. Thus the triple scattered wave is given by:

$$\psi_{\mathbf{0ab}}(\hat{\mathbf{R}}) = \frac{e^{ikR}}{R} e^{i\mathbf{k}_{in}\cdot\mathbf{0} - ik\hat{\mathbf{R}}\cdot\mathbf{0}} \frac{e^{ika - ik\hat{\mathbf{R}}\mathbf{a}}}{a} \frac{e^{ikb - ik\hat{\mathbf{R}}\mathbf{b}}}{b}$$

$$\times \mathbf{f}^T_{\mathbf{k}_{in}\hat{\mathbf{a}}} \mathbf{\Phi}_{\mathbf{k}_{in}\mathbf{ab}} \mathbf{F}_{\mathbf{a}\hat{\mathbf{b}}} \mathbf{\Phi}_{\mathbf{ab}\hat{\mathbf{R}}} \mathbf{f}_{\mathbf{b}\hat{\mathbf{R}}}.$$

The qualitative advantage of this formulation is the separation of amplitude and phase terms. The "amplitude" terms do ultimately reduce to a complex number, but its phase is roughly constant, approximately indepen-

dent of both wave number and surface structure (see however Ref. 19). The "phase" terms have phases which depend linearly on electron wave number, the constant of proportionality being the geometrical path length for this wave. The sensitivity of electron scattering to surface structure can be directly traced to the dominance of these geometrical phase terms.

The computational advantage of this formulation of the multiple-scattering problem lies in the separation of the sums on orbital angular momentum, contained in the various scattering factor matrices. The calculation of the elements of these scattering matrices requires work proportional to l_{max}, which is proportional to k. Thus for small, fixed τ, the computations are proportional to k (the square root of energy), rather than at least the fourth power of k (the square of energy) as more conventional methods demand. Furthermore, the value of τ required for a given level of numerical accuracy is a strong function of angle and scattering distance. In fact, only nearest-neighbor atoms and scattering events with small scattering angles require the terms with $\tau > 0$. For higher energies, the cone of angles which require higher order treatment becomes more and more narrow.

IV. INTERFERENCE AND GEOMETRICAL PATH LENGTH DIFFERENCES.

Having derived in the previous section expressions for the scattered wave amplitude, including curved wave multiple-scattering, we now concentrate solely on the phase of these waves. The energy dependent oscillations of the MEED curve are dominated by the geometrical phase shift terms and our discussion will ignore the rather constant phase of the "amplitude" terms

(scattering matrices) in this section.

In general, the surface may have any ordered or disordered structure. In the disordered case, diffuse electron diffraction intensities can be calculated, just as the photoelectron diffraction intensities are calculated in any detector direction. We shall, however, concentrate here on simple ordered structures with one atom per two-dimensional unit cell and upon specular reflection.

All of the scattered waves emanating from the cluster tree whose root is $\mathbf{0}_\gamma$ in layer γ sum to

$$\Psi_\gamma = \psi_{\mathbf{0}_\gamma} + \sum_{|\mathbf{a}|\neq 0} \left(\psi_{\mathbf{0}_\gamma \mathbf{a}} + \sum_{|\mathbf{b}|\neq 0} \left(\psi_{\mathbf{0}_\gamma \mathbf{ab}} + \ldots \right) \right)$$

and the complete scattered wave is

$$\Psi_s = \sum_\gamma \Psi_\gamma .$$

To see the role of two dimensional symmetry we write

$$\mathbf{0}_\gamma = \alpha \mathbf{u} + \beta \mathbf{v} + \mathbf{w}_\gamma$$

where α and β are integers, $\mathbf{u}$ and $\mathbf{v}$ are surface net lattice vectors and $\mathbf{w}_\gamma$ gives the position of the 2-D net containing $\mathbf{0}_\gamma$ for $\alpha = 0, \beta = 0$. The vectors $\mathbf{u}$ and $\mathbf{v}$ have no component normal to the 2-D net, but $\mathbf{w}$ may have x and y components to accommodate offset nets. Then

$$\Psi_s = \frac{e^{ikR}}{R} \sum_{\alpha=-N}^{N} \sum_{\beta=-N}^{N} e^{i(\mathbf{k}_{in} - k\hat{\mathbf{R}})\cdot(\alpha \mathbf{u} + \beta \mathbf{v})} \sum_{\gamma=1}^{\infty} e^{i(\mathbf{k}_{in} - k\hat{\mathbf{R}})\cdot \mathbf{w}_\gamma}$$
$$\times \left(f_{\mathbf{k}_{in}\hat{\mathbf{R}}} + \sum_{|\mathbf{a}|\neq 0} e^{ika - ik\mathbf{a}\cdot\hat{\mathbf{R}}} \frac{\mathbf{f}^T_{\mathbf{k}_{in}\hat{\mathbf{a}}} \mathbf{\Phi}_{\mathbf{k}_{in}\mathbf{a}\hat{\mathbf{R}}} \mathbf{f}_{\mathbf{a}\hat{\mathbf{R}}}}{a} \right.$$
$$\left. + \sum_{|\mathbf{a}|\neq 0} \sum_{|\mathbf{b}|\neq 0} e^{ika - ik\mathbf{a}\cdot\hat{\mathbf{R}}} e^{ikb - ik\mathbf{b}\cdot\hat{\mathbf{R}}} \frac{\mathbf{f}^T_{\mathbf{k}_{in}\hat{\mathbf{a}}} \mathbf{\Phi}_{\mathbf{k}_{in}\mathbf{ab}} \mathbf{F}_{\mathbf{a}\hat{\mathbf{b}}} \mathbf{\Phi}_{\mathbf{ab}\hat{\mathbf{R}}} \mathbf{f}_{\mathbf{b}\hat{\mathbf{R}}}}{ab} \right).$$

This organization emphasizes the accumulation of phase with scattering order. All atoms within a tree have the phase of the root atom, $\mathbf{0}_\gamma$. Each

scattering event adds a phase $kr(1-\cos\theta_{rR})$ where r is the length of the tree branch and θ_{rR} is its angle with the detector position. The intensity on a sphere at a radius R far from the diffracting surface can consequently be written as:

$$I \propto \sum_{\alpha\beta}\sum_{\alpha'\beta'} e^{i(\mathbf{k}_{in}-k\hat{\mathbf{R}})\cdot(\alpha-\alpha')\mathbf{u}}\, e^{i(\mathbf{k}_{in}-k\hat{\mathbf{R}})\cdot(\beta-\beta')\mathbf{v}} \times (I_0 + I_{\text{Bragg}} + I_{\text{ARPEFS}} + I_{\text{comb.}} + I_{\text{SSS}} + I_{\text{SSD}})\,.$$

The two dimensional sums on α, β, α', and β' lead to the two dimensional Bragg condition for diffraction spots. In the following we will assume that these Bragg conditions are met and that we are calculating the intensity of a particular diffraction spot. We have grouped the cross-terms into six categories according to the geometrical dependence of the oscillating frequency of each term with electron wave number. Table I compares these terms and explicit formulae are given below.

We group these six categories into three pairs. The first two terms, I_0 and I_{Bragg}, are the kinematic or single-scattering terms. The second pair, I_{ARPEFS} and $I_{\text{comb.}}$, arise from interference between single scattered and multiple scattered waves. The final pair, I_{SSS} and I_{SSD}, contain all interferences between multiple-scattered waves. Within each of these pairs, the first term corresponds to interference between scattered waves with trunk atoms in the same layer, while the second term corresponds to interference between waves with trunk atoms in different layers. The six intensity contributions are:

1. I_0, the atomic partial cross-sections,

$$I_0 = \sum_{\gamma=0}^{\infty} \psi_{0_\gamma}^* \psi_{0_\gamma} = \sum_{\gamma=0}^{\infty} |f_{\mathbf{k}_{in}\hat{\mathbf{R}}}^{\gamma}|^2 e^{-2k_i L_\gamma}$$

This term is the incoherent sum of the intensities of the individual scattered waves. It will vary with incident angle $\mathbf{k}_{in}$ and exit angle $\hat{\mathbf{R}}$, but it is independent of bond angles and distances. We have written complex k as $k = k_r + ik_i$ and $L_\gamma = (\hat{\mathbf{k}}_{in} - \hat{\mathbf{R}}) \cdot \mathbf{w}_\gamma$ as the path length through the material to the γ^{th} layer.

2. I_{Bragg}, leading to the weak third Bragg condition of electron diffraction,

$$\begin{aligned} I_{\text{Bragg}} &= \sum_{\gamma=0}^{\infty} \psi_{0_\gamma}^* \sum_{\gamma' \neq \gamma}^{\infty} \psi_{0_{\gamma'}} \\ &= 2\text{Re} \sum_{\gamma=0}^{\infty} e^{-2k_i L_\gamma} \sum_{\gamma' \neq \gamma} e^{ik(\hat{\mathbf{k}}_{in} - \hat{\mathbf{R}}) \cdot (\mathbf{w}_\gamma - \mathbf{w}_{\gamma'})} f_{\mathbf{k}_{in}\hat{\mathbf{R}}}^{\gamma *} f_{\mathbf{k}_{in}\hat{\mathbf{R}}}^{\gamma'} \end{aligned}$$

This term contains the interference between scattered waves from trunk atoms in different layers and modulates I_0 according to the Bragg condition for the direction perpendicular to the surface.

3. I_{ARPEFS}, the ARPEFS-like term,

$$\begin{aligned} I_{\text{ARPEFS}} &= 2\text{Re} \sum_{\gamma=0}^{\infty} \psi_{0_\gamma}^* \sum_{|\mathbf{a}| \neq 0} \psi_{0_\gamma \mathbf{a}} \\ &= 2\text{Re} \sum_{\gamma=0}^{\infty} e^{-2k_i L_\gamma} \sum_{|\mathbf{a}_\gamma| \neq 0} e^{ik\mathbf{a}_\gamma - ik\mathbf{a}_\gamma \cdot \hat{\mathbf{R}}} \\ &\quad \times f_{\mathbf{k}_{in}\hat{\mathbf{R}}}^{\gamma *} \frac{\mathbf{f}_{\mathbf{k}_{in}\hat{\mathbf{a}}}^{T} \Phi_{\mathbf{k}_{in}\mathbf{a}\hat{\mathbf{R}}} \mathbf{f}_{\mathbf{a}\hat{\mathbf{R}}}}{a} \end{aligned} \tag{4}$$

This contribution to the intensity arises from interference between single scattering from a trunk atom and multiple scattering from atoms within that same tree. As we shall see, this term gives rise to the

majority of the "extra" peaks in intensity curves. The oscillation frequencies present in this term are of the same form as found in ARPEFS and the path length differences in the phase of I_{ARPEFS} are the same as in Eq. 2. The path-length differences are equal to the lengths of tree branches, plus the emission direction dependent path $\mathbf{a}_j \cdot \hat{\mathbf{R}}$.

4. $I_{\mathrm{comb.}}$, the combination term,

$$I_{\mathrm{comb.}} = 2\mathrm{Re} \sum_{\gamma=0}^{\infty} e^{-2k_i L_\gamma} \sum_{\gamma' \neq \gamma} e^{ik(\hat{\mathbf{k}}_{in} - \hat{\mathbf{R}}) \cdot (\mathbf{w}_\gamma - \mathbf{w}_{\gamma'})} \sum_{|\mathbf{a}_\gamma| \neq 0} e^{ika_\gamma - ik\mathbf{a}_\gamma \cdot \hat{\mathbf{R}}} f^{\gamma' *}_{\mathbf{k}_{in}\hat{\mathbf{R}}} \frac{\mathbf{f}^T_{\mathbf{k}_{in}\hat{\mathbf{a}}} \Phi_{\mathbf{k}_{in}\mathbf{a}\hat{\mathbf{R}}} \mathbf{f}_{\mathbf{a}\hat{\mathbf{R}}}}{a}$$

This intensity arises when a single-scattered wave from a trunk atom in one layer interferes with multiple scattered waves from trees rooted in a different layer. The oscillation frequencies in this term will be combinations of the frequencies in I_{Bragg} and I_{ARPEFS}: the path length differences will be equal to the length of a tree branch plus the emission direction dependent path $\mathbf{a}_j \cdot \hat{\mathbf{R}}$ minus the offset of the two trunk atoms along the incident and exit directions.

5. I_{SSS}, where SSS stands for "scattered-wave, scattered-wave same": this term includes all interference between multiple scattered waves originating from trunk atoms in the same layer. We shall not give an explicit formula as it is not very illuminating. This term contains frequencies equal to differences between pairs of frequencies appearing in I_{ARPEFS}, in other words frequencies equal to differences in the lengths of tree branches.

6. I_{SSD}, interference between multiple scattered waves with trunk atoms

in different layers. This term is similar to I_{SSS}, but the displacement between the trunk atoms leads to path length differences which contain added or subtracted Bragg components depending on the relative z component of the trunk atoms.

These six "intensities" are not physically separable and they might also be called "interferences" since they need not be positive.

This decomposition helps to focus on the nature of the structure information in MEED. It is important to recognize that we have included all contributions to the MEED intensity. Thus, even including curved-wave and multiple-scattering effects, we can always write the MEED curve in a form directly analogous to the ARPEFS form of Eq. 1:

$$\frac{I_{MEED} - I_0}{I_0} = \chi_{MEED} = \sum_j A_j(k) \cos[kp_j + \phi_j(k)]$$

where A_j is the amplitude and ϕ_j is the phase of the product of two or more scattering factors and the path length differences p_j are given by

$$p_j = \pm 2d_\perp \cos\alpha + \sum_{j'} r_{j'}(1 - \cos\theta_{r_{j'}\hat{\mathbf{R}}}). \tag{5}$$

Here $d_\perp$ is some interlayer spacing, α is the angle between incident beam direction and the surface normal, and $r_{j'}$ is the bond vector between some pair of atoms in the surface. In other words, *the MEED intensity is a cosine series whose frequencies are equal to either Bragg path length differences, ARPEFS-like path length differences, or to a combination of these differences.* This conclusion is a result of the scattering interference geometry alone. Specifically, it does not depend upon our particular method of calculating the scattering factors, or upon the multiple-scattering order, or upon

the surface ordering or, in fact, upon the energy range of the scattering events.

For this conclusion to be useful for understanding the MEED intensity, the functions A_j and ϕ_j must not be strong functions of k and the total number of different scattering interferences must not be overwhelmingly large. These criteria are only partially satisfied in the medium energy range. In the lower energy range, these criteria may not be satisfied at all even with the simplest surface structures. Before exploring the application of this analysis to MEED, we shall discuss the numerical convergence of our calculations in the next section.

V. CONVERGENCE

In this section we shall describe the convergence of the MEED specular (00) beam intensity as a function of the number of scattering events and of the Taylor series order.

We control the number of scattering events in two separate ways. First, for each scattering event, the scattering amplitudes for the required angles are estimated using the maximum plane wave scattering amplitude over the chosen energy range. This estimate is compared to an amplitude cutoff criterion to select only large scattering amplitude events. For the events actually calculated, we find our estimates to be between 50% too high and 20% too low. Second, we limit the total path length between the trunk atom and any scattering atom at the ends of the tree. Note that we specifically do not limit the order of the multiple-scattering perturbation series because, in fact, multiple forward scattering is never small in the MEED energy range.

The convergence in scattering amplitude cutoff is illustrated in Fig. 2. Starting with an amplitude just above convergence, the cutoff amplitude was successively reduced by a factor of 2 to yield the three MEED curves shown. The inset figure illustrates the convergence in multiple-scattering order. The energy range we have chosen here (100-550eV, corresponding to 5-12Å^{-1} wave numbers) should be a very demanding test of the convergence of our method.

The convergence in the path length difference cutoff is similar, with a cutoff around 13.5Å being adequate to give the dominant MEED features.

The Taylor series order convergence is illustrated in Fig. 3. The zero order curve is remarkably good for Ni, suggesting that this very simple theory may be useful for structure screening in the initial stages of a structure determination. The first and second order curves are nearly identical, demonstrating convergence in scattering at first order in this case. This rapid convergence in scattering order is in agreement with corresponding observations in ARPEFS.[17]

VI. PATH LENGTH DIFFERENCE ANALYSIS FOR CLEAN FCC (001) SURFACES.

Now we wish to explore systematic features of MEED intensities for clean fcc metal surfaces with the help of our analysis method. We shall divide our discussion into two parts. In the first part we analyze the features of the MEED curve for near normal incidence on the (001) face of an ideally terminated fcc metal. In the second part we move the angle of incidence away from normal and follow the changes in the character of the curves.

A. MEED specular intensity for fcc (001) surface.

We begin with the intensity dependence on wave number of the MEED (00) beam for 4° off-normal angle of incidence, using Ni as an example, but we limit our discussion to those features shared by all fcc metals. We have selected this special case to help establish a connection between our analysis and the analysis applied to LEED.

1. $I_0 + I_{\text{Bragg}}$

In Fig. 4 we have superimposed the $I_0, I_0 + I_{\text{Bragg}}$, and the full I_{MEED} curves. The I_0 curve is simply the backscattering cross-section for Ni atoms. The $I_0 + I_{\text{Bragg}}$ curve is the single-scattering (kinematic) result. A typical interference leading to these oscillations is shown in Fig. 5(a). The regular spacing of the crystal layers leads to a phase relation between the interference oscillations in I_{Bragg}which gives rise to Bragg peaks.

We can associate the Bragg peaks with peaks in the I_{MEED} curve of Fig. 4, but the MEED peaks are shifted and altered in amplitude, and some additional peaks appear between the Bragg peaks. We look to multiple-scattering effects to describe the extra features and the modification of the Bragg peaks.

2. I_{ARPEFS}

The primary multiple-scattering in MEED is forward scattering in a narrow cone with width of the order of 10°-20°. Consequently, for near normal incidence on an ABAB... stacked fcc surface, the major forward scattering events occur between alternate layers, i. e. between even-numbered or be-

tween odd-numbered layers (see Fig. 5(b)). When these waves interfere with the trunk atom scattering, the characteristic frequency will be given by the path length difference between the alternate layers, i.e. four times the interlayer spacing counting the two layer spacings going down and two going up. This is very close to twice the frequency of the Bragg peaks (interference between every layer) because the incidence angle of 4° is so close to normal. These interferences belong to I_{ARPEFS} which is therefore dominated by an oscillation with twice as many peaks as I_{Bragg}, as illustrated in Fig. 6 (compare with Fig. 4). Half of the peaks in I_{ARPEFS} lie near Bragg peaks but the other half lie approximately halfway between the Bragg peaks and can be clearly associated with I_{ARPEFS}. This explains the majority of the extra features in the MEED curve. For an fcc(111) surface with ABCABC... stacking one would obtain extra peaks at approximately the one-third and two-thirds positions between the Bragg peaks.

Such peaks have often been observed (and calculated) in LEED, especially at higher energies, but have never been explained in a simple way up to now. These features have been labeled[20] "secondary Bragg peaks", but this obscures their local, multiple-scattering origin. The frequency of these oscillations will not follow the Bragg law: the corresponding path length difference is independent of the incident angle.

We note that the maxima in I_{ARPEFS} occur at wave numbers slightly less than k_{Bragg}. This is a result of the two extra phase shifts which accompany the multiple-scattering events. First, there is an extra scattering phase shift when the electron wave is forward scattered: it is a large, mostly constant shift to lower wave number. The second phase shift is geometrical: the

multiple-scattering path length for forward scattering is always equal to or greater than the path which passes straight through. It always shifts the interference to lower wave numbers.

3. $I_{\text{comb.}}$

When a multiple-scattered wave interferes with single-scattered waves in other layers, an interference oscillation with a combined Bragg-like and ARPEFS-like frequency arises (see Fig. 5(c)), which we call $I_{\text{comb.}}$. For a truncated bulk fcc metal, the $I_{\text{comb.}}$ intensity has large-amplitude features when $k = k_{\text{Bragg}}$, but the intensity of the features is modulated by an ARPEFS-like oscillation. As described above, the oscillations in I_{ARPEFS} lag behind the Bragg peaks. In fact, the lag is more than $\pi/2$ for Ni atoms at 4° incidence: the ARPEFS oscillation is in its negative cycle near k_{Bragg} and the features in $I_{\text{comb.}}$ are therefore large *negative* spikes as shown in Fig. 7. Recall that $I_{\text{comb.}}$ and the other "intensities" are actually interference terms: only their sum must be positive. Thus the multiple-scattering tends to destructively interfere with the single-scattering, reducing the size of the Bragg peaks.

4. I_{SSS} *and* I_{SSD}

The strong backscattering power of Ni ensures that the interference structure of 4° incidence is dominated by single-scattering interference with single- or multiple-scattering. Thus for qualitative analysis of the near-normal incidence curve we may ignore I_{SSS} and I_{SSD}. In the next section we will encounter scattering geometries in which the multiple-scattering to

multiple-scattering interference becomes more important.

B. Incidence Angle Dependence of the (00) beam intensity

We shall examine the changes in the MEED curve and its components as the incidence angle increases from 4° to 44° in an azimuth containing a [011] direction.

We must start with an examination of the scattering properties of Ni. Fig. 8 shows the angular dependence of the scattering power for Ni at two wave numbers, 6.5Å^{-1} (161eV) and 10.5Å^{-1} (420eV). The substantial conclusions of this section can be deduced from a careful comparison of the angle dependence of the scattering power to the scattering geometry. A strong forward peak dominates these curves, becoming more pronounced at higher energy. A second lobe occurs for 180° backscattering. Also note two low points, at approximately 70° and 120–130°.[19] Marked on Fig. 8 are the scattering angles $\theta = \pi - 2\alpha$ for incident angles α. We can anticipate that the amplitude of the single-scattered waves will decrease significantly for $60° > \alpha > 12°$, i. e. for $60° < \theta < 156°$.

The MEED curves for six incidence angles α between 4° and 44° are shown in Fig. 9. We shall analyze these curves by decomposing them by the method of the preceding section. The salient features we must account for are i) the persistence of Bragg-like features for all angles as indicated by the peaks near the Bragg condition markers in Fig. 9 and ii) the introduction of additional features, particularly at low energies, as we approach the largest incidence angle plotted.

We start with the Bragg-like features. The curves all have a peak near

the position expected for interference between single-scattered waves from each layer, but many of these apparent Bragg peaks are *not* "kinematic". Fig. 10 shows I_0+I_{Bragg} for the same conditions as Fig. 9. For the angles 20°, 28°, and 36°, the small scattering power of Ni atoms at high energy for the angle $\pi - 2\alpha$ means that single-scattering is very weak. All of the interference features involving single-scattered waves, namely $I_0, I_{\text{Bragg}}, I_{\text{ARPEFS}}$, and $I_{\text{comb.}}$, will thus be small. Multiple collision paths can, however, enter the detector via paths that do not involve scattering through the angle $\pi - 2\alpha$: they can have significant amplitude even when single scattering is small. Thus the majority of the intensity in the higher energy region for the angles 20°-36° must originate from interference between multiple-scattering waves, i. e. either I_{SSS} or I_{SSD}.

For I_{SSS}, the path length differences must themselves be differences between pairs of ARPEFS-like path length differences. Thus the Bragg-like multiple-scattering features cannot be primarily due to I_{SSS}; they must arise from I_{SSD}. As shown in Fig. 12, the I_{SSD} term leads to Bragg-like features for all incidence angles (excepting only the highest energy Bragg condition in the 36° curve).

The second characteristic of the angle dependence which we would like to understand is the additional features which seem to grow in at lower energies and higher angles. The appearance of new features coincides with the return of the Bragg peaks in Fig. 10, suggesting that in part they originate from an increase in the single scattered waves. However, the Bragg peaks for 44° incidence are weaker and wider than at 4° because fewer layers contribute at a more grazing angle. Attenuation of the Bragg peaks highlights the

I_{ARPEFS} oscillations, which need not be weaker at 44° than at 4°: Fig. 11 shows the I_{ARPEFS} features on the same scale as Fig. 9.

The attenuation of the Bragg features also helps the visibility of the I_{SSD} features. As we can see from Fig. 12, the I_{SSD} peaks still have Bragg-like peaks, but additional, higher frequency oscillations are nearly as large. These extra oscillations represent interferences whose periodic extensions have been attenuated by long path lengths. This truncates the Bragg sum leaving a cosine oscillation. Furthermore, the 44° geometry allows multiple forward scattering to occur for every layer, rather than every other layer as we saw for 4°. Thus the Bragg-like peaks in I_{SSD} for 44° are shifted far enough away from the real Bragg peaks to give separate structures in the MEED curve. To summarize the character of the 44° spectrum we can say that the increase in the number of features follows from a more even balance of multiple-scattering and single scattering (Bragg) features, combined with the larger shift of the I_{SSD} peaks leading to two separate sets of Bragg-like peaks, one kinematic and one due solely to interference between multiple-scattering waves.

VII. COMPARISON WITH OTHER METHODS FOR MEED COMPUTATION

As discussed in the introduction, several methods have been proposed to overcome the barrier to MEED intensity computations. Our approach in this paper is rather different in that we have no direct connection to any particular organization of the crystal and we use a different mathematical formulation of the individual scattering events.

The cluster LEED theories are similar in spirit to our cluster MEED theory, in that periodicity is partly or wholly abandoned. However, different formulations of the individual scattering events are appropriate to low and to medium energies. This also applies to the RHEED-like theory of MEED.[16] Its use of a plane-wave representation of atomic scattering leads to plane-wave scattering factors. The generalized scattering factors we employ reduces to plane-wave limits for large scattering distance and, presumably, large energy.

Similar methods for computing individual scattering events based on rotated coordinate systems have been suggested.[21,22] While these computational methods have not been adapted for MEED, our work here shows that such an extension is possible.

We should note that our present method is not restricted in incidence angle or energy in principle, but we are limited at low energy and high angle by the possibility of resonant scattering and at very high energy because the computations are still proportional to the number of phase shifts $l_{\max} \approx kr_0$.

Fig. 13 compares the new calculation method with a traditional LEED calculation for an angle of incidence that shows high sensitivity to convergence. The discrepancies in peak heights can be traced to incomplete convergence at the low energies used here. Our current programs require about 6 sec of VAX 8650 CPU time per energy point for the interval of Fig. 13, compared with about 9 sec for a standard non-symmetrized LEED program. The big gain shows up at higher energies: the computational effort of the present method only triples from 100eV to 1000eV, while the standard LEED calculation will have increased by two orders of magnitude.

VIII. CONCLUSIONS

We have presented two developments in the theory of medium energy electron diffraction. The first is computational: the efficient TS-MQNE method for multiple-scattering has been adapted for electron diffraction. The second is conceptual: we have analyzed the multiple-scattering part of MEED in terms of individual scattering paths.

The computation of MEED intensities by the method we describe here is much more effective than the methods used for LEED whenever the scattering energy or the unit cell size is large. We do not claim that our method is as yet the optimal one. But we have reduced the power of the functional dependence of the computations on energy from square to square root. Further improvements seem possible. In particular, at some high energy the Born approximation will be useful, as in RHEED. Then the computations would become independent of energy using our cluster scheme.

A clean low-Miller-index fcc metal surface is a worst-case choice to exhibit the advantages of our method, especially with respect to unit cell size. On the other hand, our method scales only linearly with the number of atoms in the unit cell rather than proportionally to the fourth or higher power of that number, as with conventional LEED methods. Thus our method has its greatest potential in solving complex surface structures, whether ordered or disordered.

Our second contribution in this paper is a different perspective on the electron diffraction problem, one which emphasizes the individual electron-atom collisions. We have made an in-depth analysis of a simple fcc metal,

demonstrating that even the multiple-scattering interference structure in the MEED curves can be connected straightforwardly to scattering events.

ACKNOWLEDGEMENTS

J.J. Barton thanks the IBM Corp. for their Postdoctoral Fellowship grant and D. A. Shirley for his support in obtaining that grant. We thank S.W. Robey for his help in generating the partial wave phase shifts for the fcc metals at medium energies. This work was supported by the U. S. Army Research Office, with institutional support at Lawrence Berkeley Laboratory by the Director, Office of Energy Research, Office of Basic Energy Sciences, Materials Sciences Division of the U. S. Department of Energy, under Contract No. DE-AC03-76SF00098.

REFERENCES

*Current Address: IBM Watson Research Center, Yorktown Heights, NY

[1]J. J. Barton, C. C. Bahr, S. W. Robey, Z. Hussain, E. Umbach, and D. A. Shirley, Phys. Rev. B **34**, 3807 (1986).

[2]P. J. Orders and C. S. Fadley, Phys. Rev. B **27**, 781 (1983).

[3]P. A. Lee, Phys. Rev. B **13**, 5261 (1976).

[4]J. J. Barton, C. C. Bahr, Z. Hussain, S. W. Robey, J. G. Tobin, L. E. Klebanoff, and D. A. Shirley, Phys. Rev. Lett. **51**, 272 (1983).

[5]J. J. Barton and D. A. Shirley, Phys. Rev. B **32**, 1906 (1985).

[6]S. Y. Tong and C. H. Li, in *Chemistry and Physics of Solid Surfaces*, edited by R. Vanselow, (Chemical Rubber Co., England, 1982), p. 287.

[7]J. J. Barton and D. A. Shirley, Phys. Rev. B **32**, 1892 (1985).

[8]M. -L. Xu, J. J. Barton, and M. A. Van Hove, Phys. Rev. B (in preparation);

[9]J. B. Pendry, *Low-Energy Electron Diffraction* (Academic Press, London, 1974).

[10]M. A. Van Hove and S. Y. Tong, *Surface Crystallography by LEED* (Springer-Verlag, Heidelberg, Berlin, New York, 1979).

[11]M. A. Van Hove, W. H. Weinberg and C.-M. Chan, *Low-Energy Electron Diffraction* (Springer-Verlag, Heidelberg, Berlin, New York, 1986).

[12]J. B. Pendry, in *Determination of Surface Structures by LEED*, edited by P. M. Marcus and F. Jona, (Plenum, New York, 1984), p. 3; F. Jona, J. A. Strozier Jr., and P. M. Marcus, in *The Structure of Surfaces*, edited by M. A. Van Hove and S. Y. Tong, (Springer-Verlag, Heidelberg, Berlin, New York, 1985), p. 92; J. B. Pendry and D. K. Saldin, Surf. Sci. **145**, 33 (1984); D. K. Saldin, D. D. Vvedensky, and J. B. Pendry, in *The Structure of Surfaces*, edited by M. A. Van Hove and S. Y. Tong, (Springer-Verlag, Heidelberg, Berlin, New York, 1985), p. 131; K. Heinz, D. K. Saldin, and J. B. Pendry, Phys. Rev. Lett. **55**, 2312 (1985).

[13]N. Bickel and K. Heinz, Surf. Sci. **163**, 435 (1985).

[14]N. Masud, C. G. Kinniburgh, and J. B. Pendry, J. Phys. C **10**, 1 (1977).

[15]P. A. Maksym and J. L. Beeby, Surf. Sci. **110**, 423 (1981).

[16]P. A. Maksym and J. L. Beeby, Surf. Sci. **140**, 77 (1984).

[17]J. J. Barton, S. W. Robey, and D. A. Shirley, Phys. Rev. B **34**, 3807 (1986).

[18]J. J. Barton and D. A. Shirley, Phys. Rev. A **32**, 1019 (1985).

[19]J. J. Barton, Z. Hussain, and D. A. Shirley, Phys. Rev. B **35**, 933 (1987).

[20]E. G. McRae, J. Chem. Phys. **45**, 3258 (1965).

[21]J. J. Rehr, J. M. de Leon, C. R. Natoli, and C. S. Fadley, J. Physique **47**, C8-213 (1986).

[22]V. Fritzsche and P. Rennert, Phys. Stat. Sol. (b) **135**, 49 (1986).

TABLE

TABLE I. Classification of MEED Interferences. All of the structure in a MEED curve orginates from interferences in one of these six categories. The characteristic path length differences Δp are given for each category.

Interference	Trunk atoms in same layer	Trunk atoms in different layers
$\psi_0^* \psi_0$	I_0 (Atomic), $\Delta p = 0$	Bragg, $\Delta p = 2d_\perp \cos\alpha$
$\psi_0^* \sum_j \psi_j$	ARPEFS, $\Delta p = a(1 - \cos\theta_{aR})$	Comb., $\Delta p = 2d_\perp \cos\alpha \pm a(1 - \cos\theta_{aR})$
$\sum_j \psi_j^* \sum_{j'} \psi_{j'}$	SSS, $\Delta p = \sum_i a_i(1 - \cos\theta_{a_i R})$	SSD, $\Delta p = 2d_\perp \cos\alpha \pm \sum_i a_i(1 - \cos\theta_{a_i R})$

FIGURE CAPTIONS

FIG. 1. Multiple-Scattering Tree. The diagram shows a cross-sectional view of a surface with an incident beam (solid line) reaching the "trunk" atom of a tree, several scattered wave propagation directions ("bond" vectors) (dotted lines) and the exiting scattered waves headed toward the detector (MEED spot) (dashed lines).

FIG. 2. Convergence of the specular (00) MEED beam intensity for electrons incident 4° from normal on a Ni (001) surface. The inset shows the number of scattering events computed for each multiple-scattering order, e.g., order 3 is triple scattering. The solid curve has the most scattering events, while the other two curves have events with amplitudes estimated to be half of the solid curve (dashed line) and one fourth of the solid curve (dot-dash line). The intensities are multiplied by k^2 to give more even values across the entire momentum range.

FIG. 3. Convergence in Taylor series parameter τ for the MEED (00) intensity for 4° incident electrons on a Ni(001) surface. The solid curve was computed with $\tau = 0$, the dashed curve with $\tau = 1$, and the dot-dash curve with $\tau = 2$. The similarity of these last two curves makes them difficult to distinguish, illustrating the convergence of the Taylor expansion.

FIG. 4. Solid curve is I_{MEED}, the full multiple-scattering curve for specular reflection from Ni(001) at 4° off-normal. Dotted curve is $I_0 + I_{\mathrm{Bragg}}$, the kinematic or single scattering result. Dash curve is I_0, the atom cross-section.

FIG. 5. Schematic illustration of three pairs of electron paths whose interference gives the dominant character of the MEED curve for near normal incidence on an fcc (001) surface. The first pair, (a), gives the Bragg-like peaks. The second pair, (b), yields ARPEFS-like oscillations. The third pair, (c), represents the only other type of interference between single- and multiple-scattering paths.

FIG. 6. Specular MEED intensity for electrons incident 4° from normal to the (001) face of a Ni surface. The solid line is the full calculated MEED curve while the dotted curve includes only interferences similar to the interference responsible for ARPEFS (I_{ARPEFS}). Bragg-like peaks occur near 7Å^{-1}, 8.75Å^{-1}, and 10.6Å^{-1}.

FIG. 7. The contribution $I_{\mathrm{comb.}}$ to the full I_{MEED}, and its relationship to $I_{\mathbf{Bragg}} + I_0$.

FIG. 8. The scattering power $|f(\theta)|$ for Ni atoms as a function of scattering angle θ at 6.5Å^{-1} (161eV) (line with circles) and 10.5Å^{-1} (420eV) (line with pluses). The scattering angles θ for various incidence angles α discussed in the text are marked by vertical bars.

FIG. 9. Calculated MEED (00) beam intensities for a range of incident polar angles in a [011] azimuth on a Ni (001) surface. The curves for angles greater than 12° have been enlarged by a factor of 3. Vertical bars mark the positions of the ideal "kinematic" Bragg peaks.

FIG. 10. Components $I_0 + I_{\text{Bragg}}$ of the MEED curves in Fig. 9. The scale has been deliberately chosen to be the same as Fig. 9 to facilitate comparison.

FIG. 11. Same as Fig. 9 except displaying I_{ARPEFS}. Note that the same scale has been used as in Fig. 9 to facilitate comparison

FIG. 12. Same as Fig. 9 except displaying I_{SSD}. Note that the same scale has been used as in Fig. 9 to facilitate comparison

FIG. 13. LEED multiple-scattering calculations for an incidence direction of (θ, ϕ)=(8°,45°) on Ni(001), (00) beam. Upper curve: method of Ref. 10. Lower curve: present work.

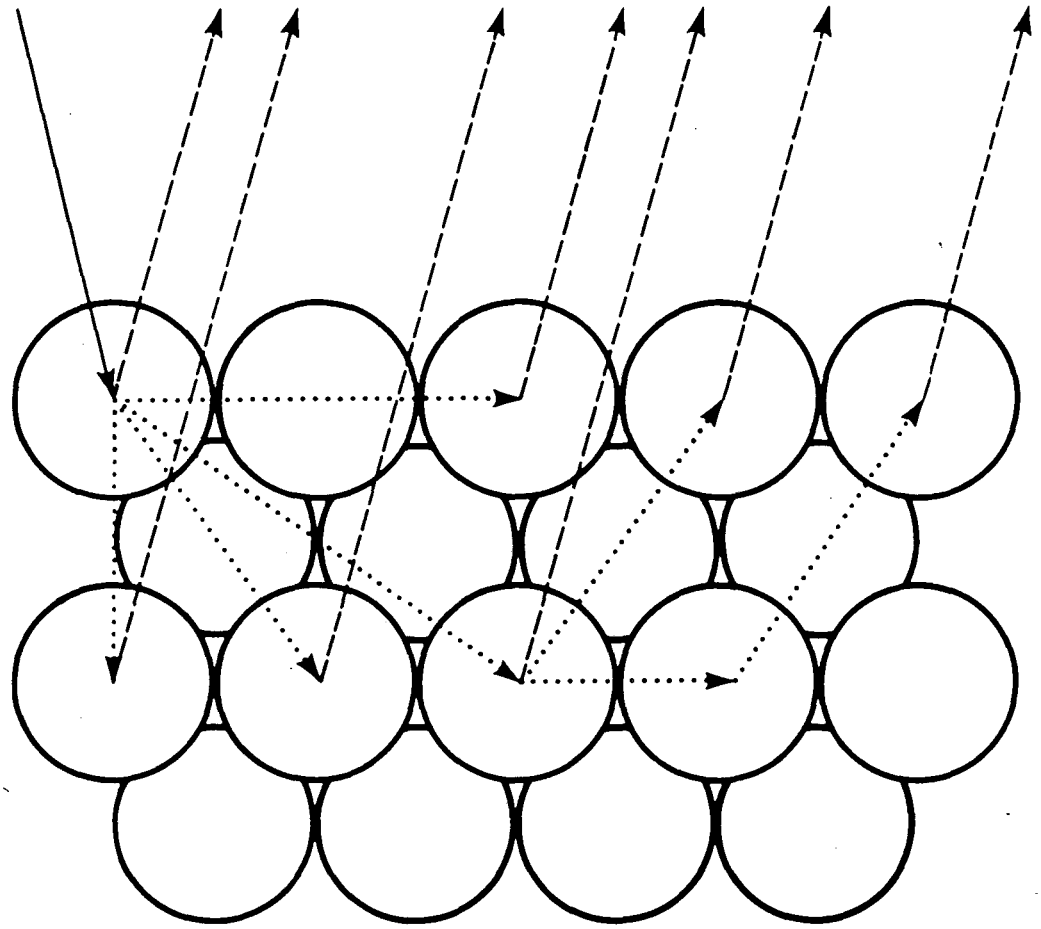

XBL 876-6329

Fig. 1

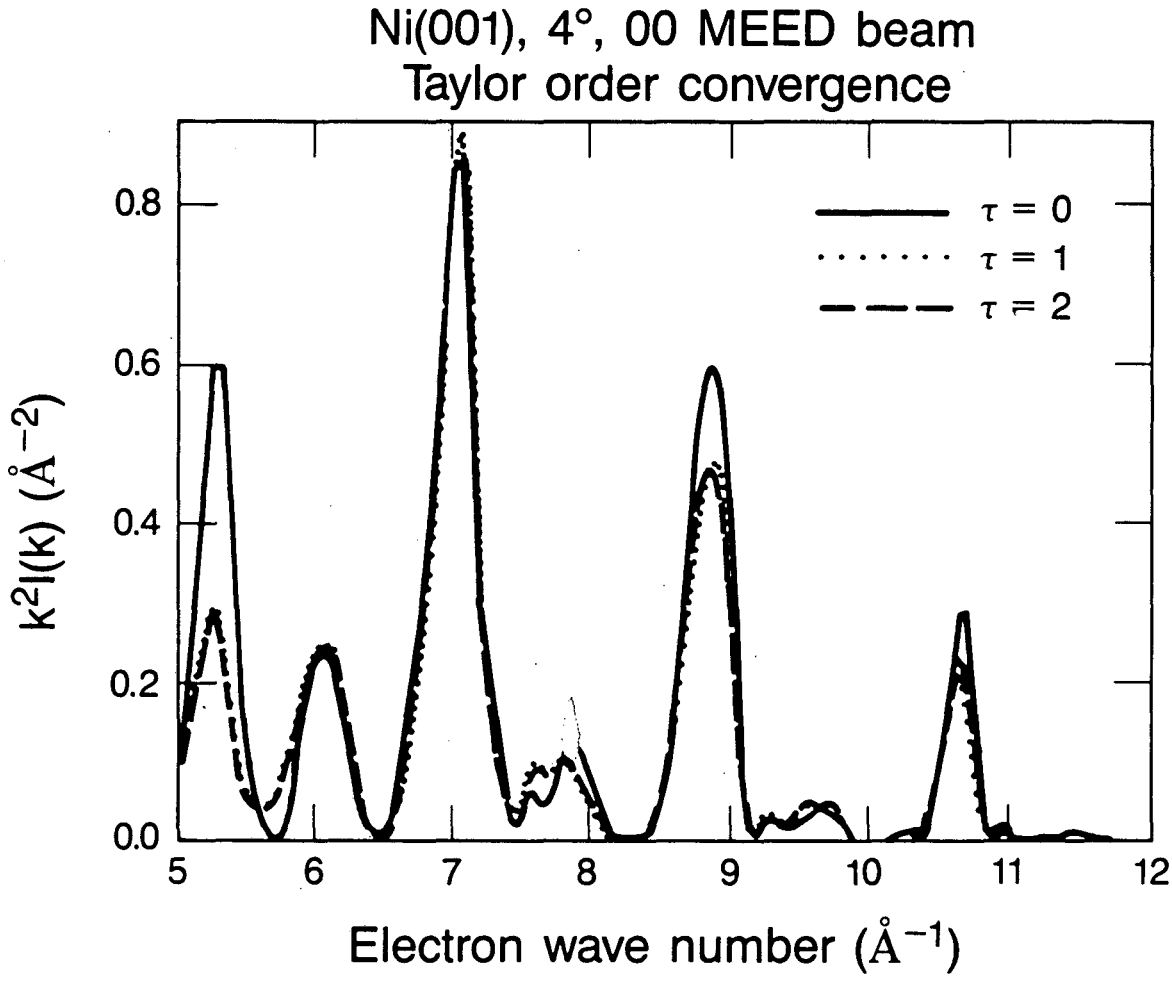
Ni(001), 4°, 00 MEED beam
Taylor order convergence
τ = 0
τ = 1
τ = 2
0.8
0.6
0.4
0.2
0.0
5
6
7
8
9
10
11
12
k²I(k) (Å⁻²)
Electron wave number (Å⁻¹)
XBL 876-6331

Fig. 2

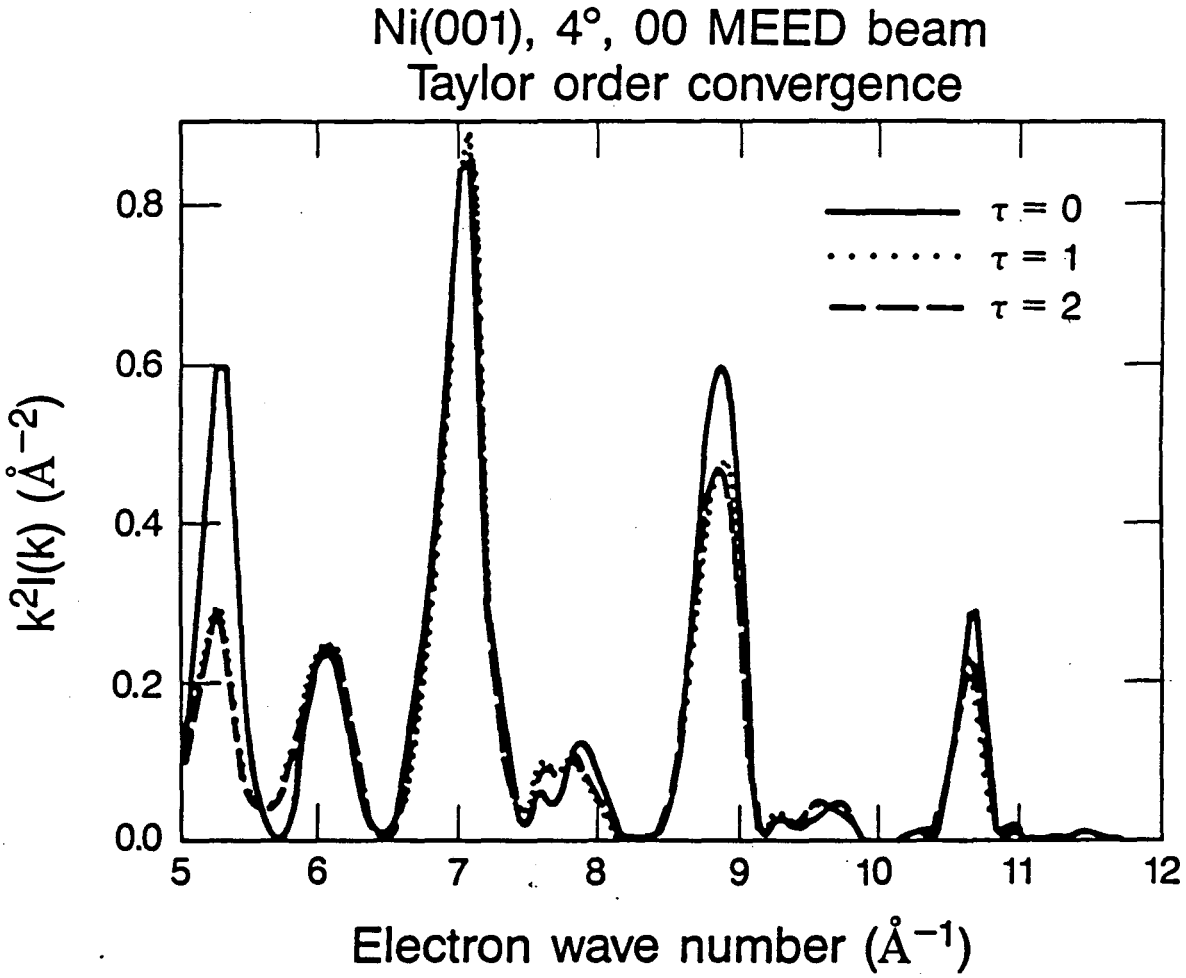

XBL 876-6331

Fig. 3

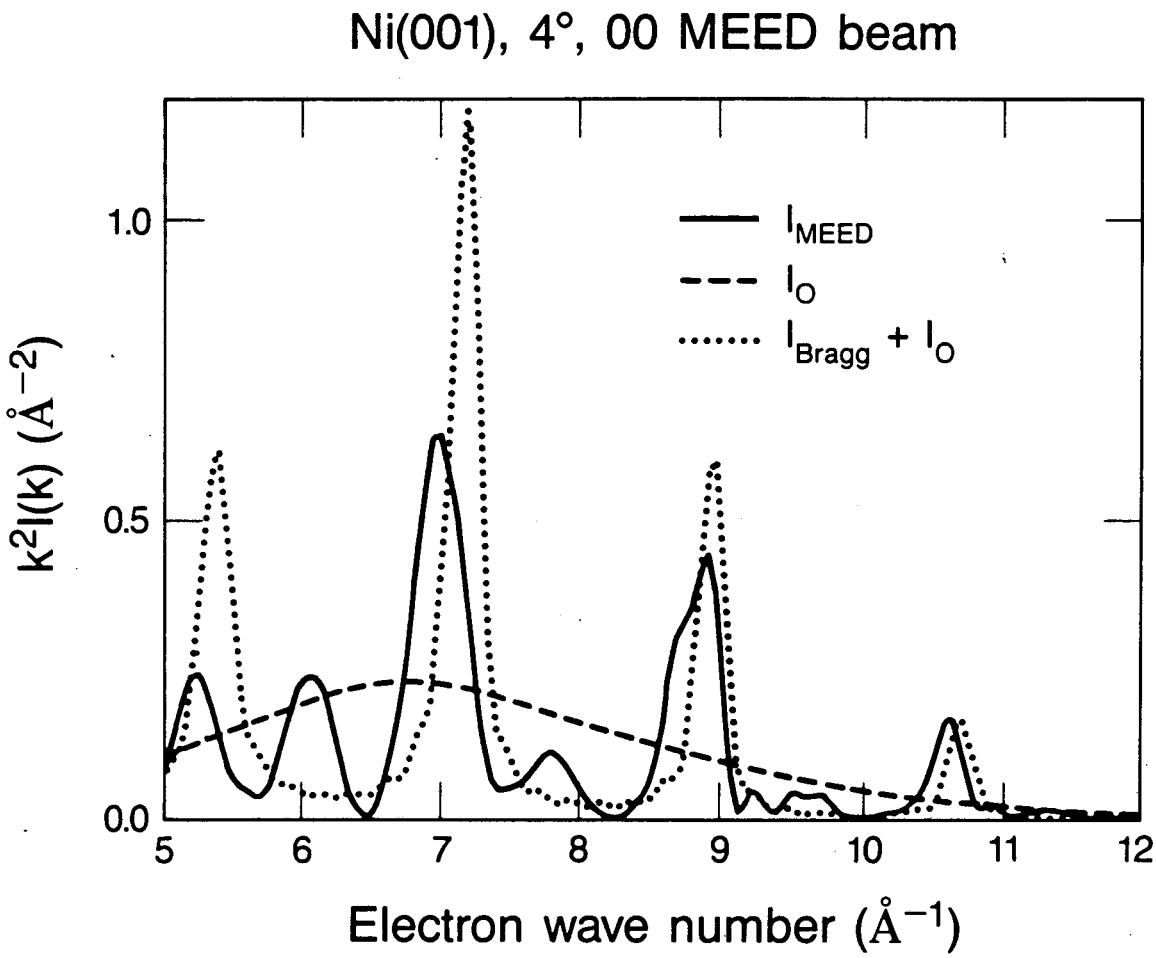

XBL 876-6334A

Fig. 4

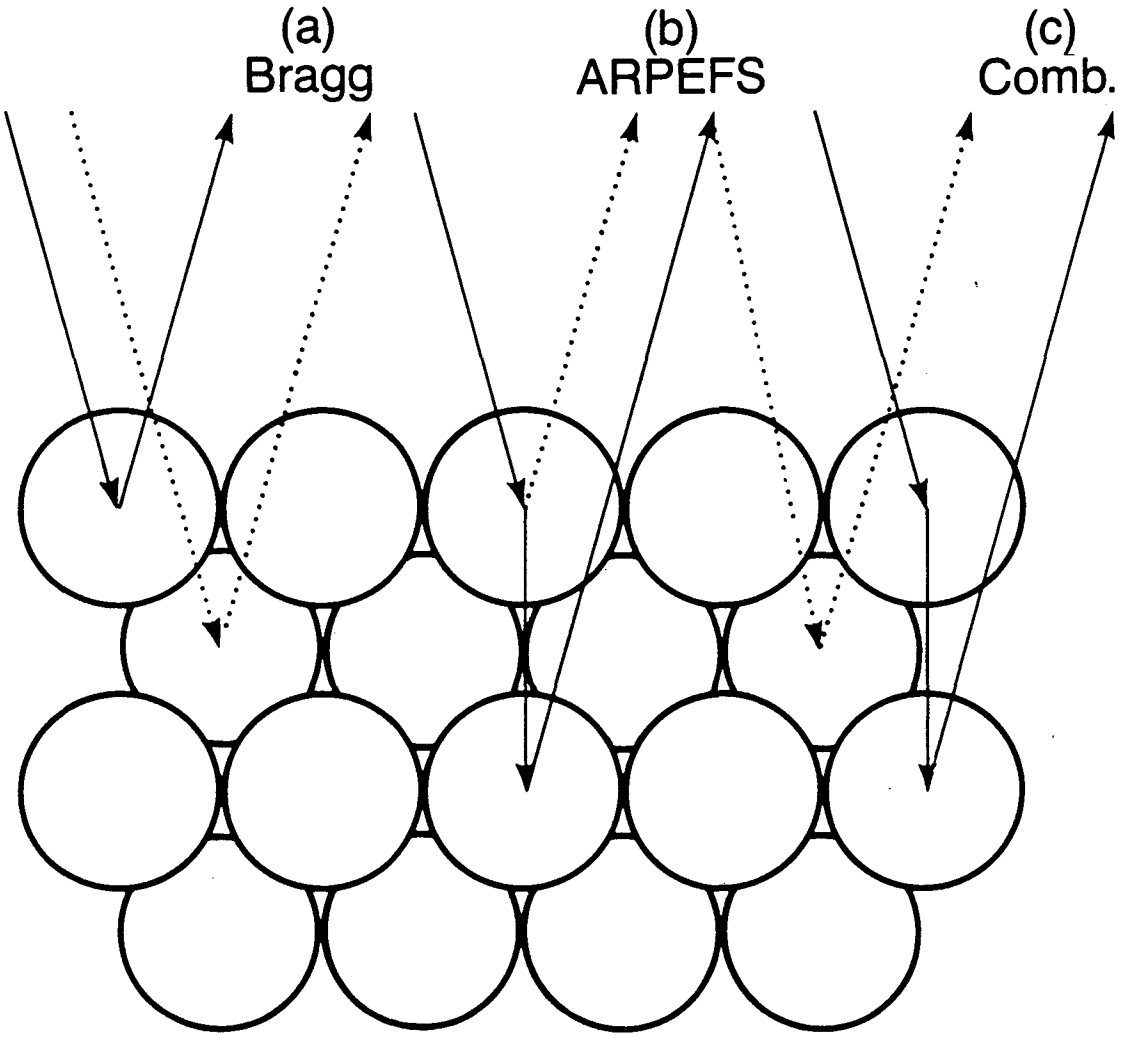

XBL 876-6328

Fig. 5

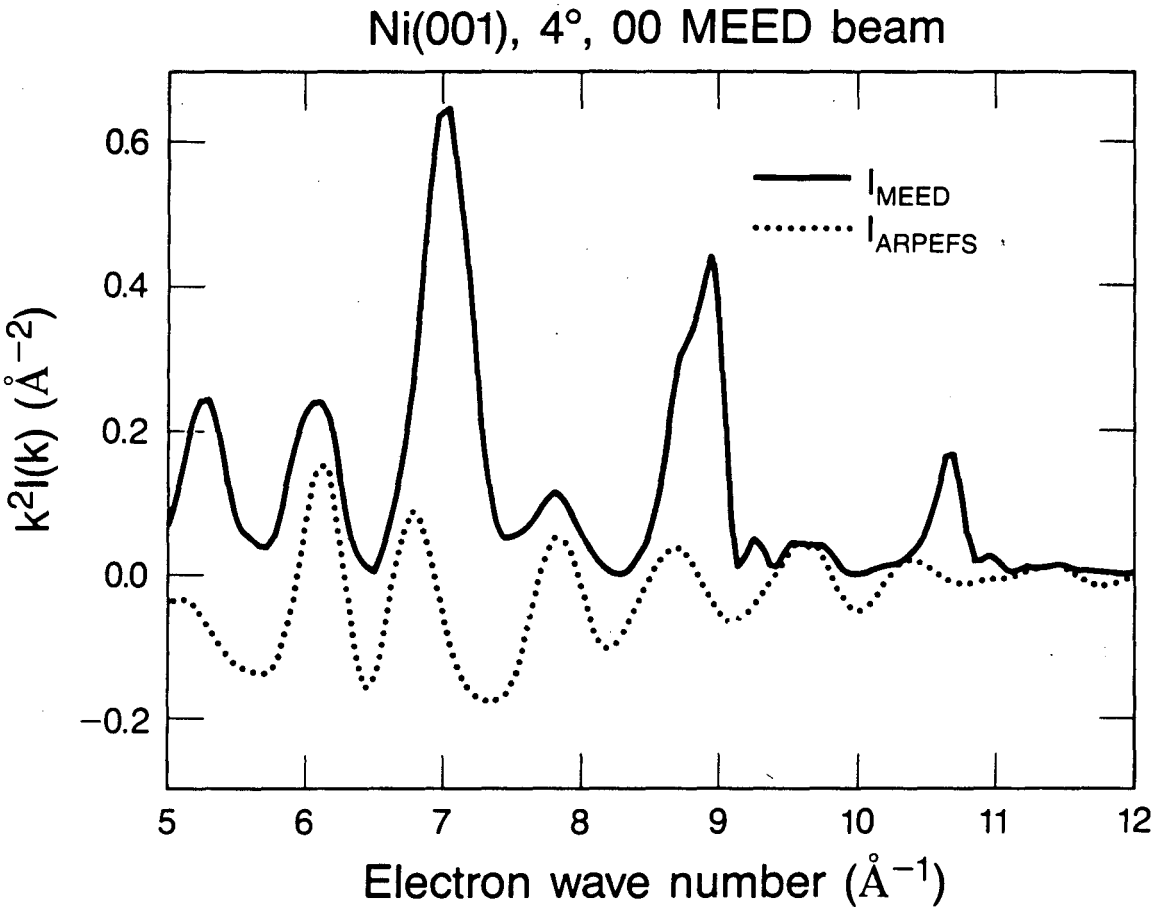

XBL 876-6332

Fig. 6

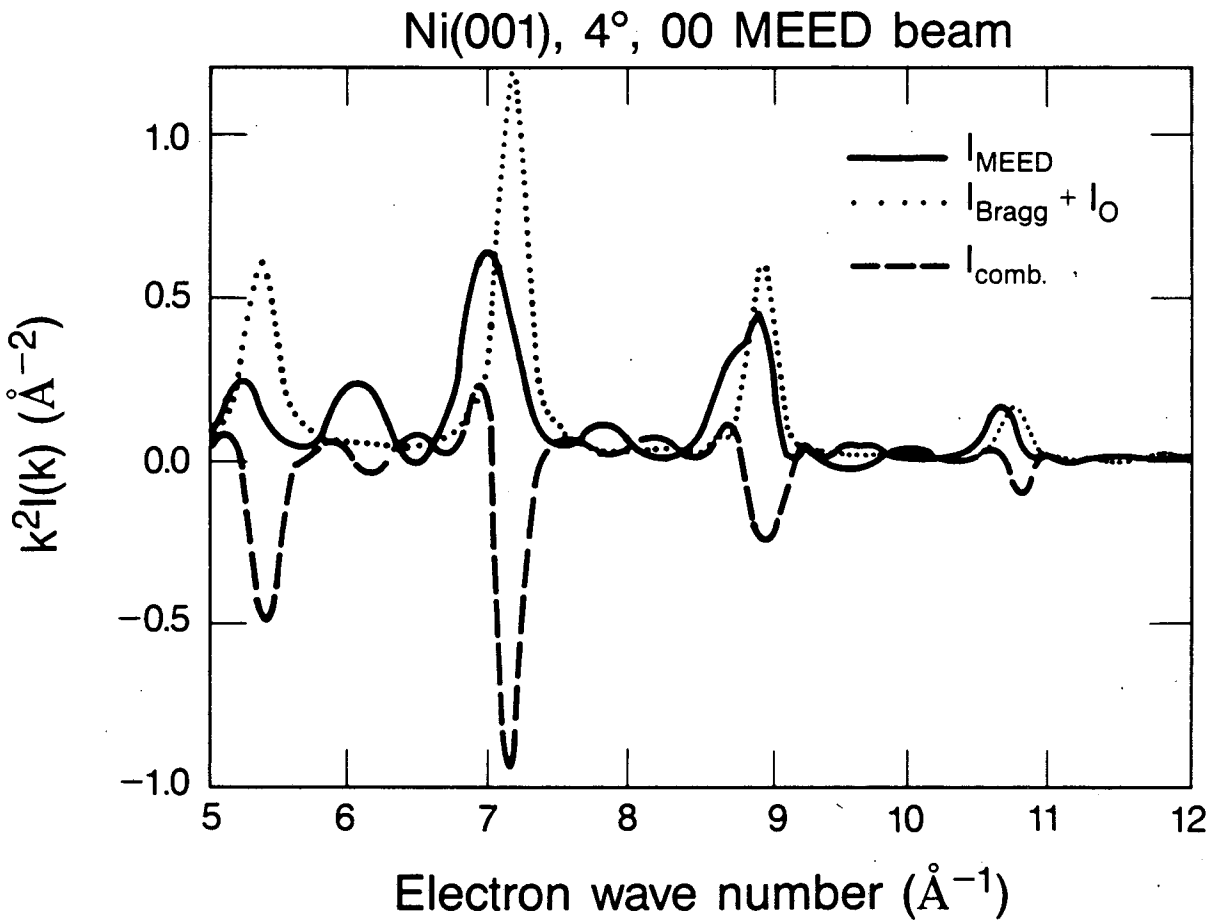

XBL 876-6330

Fig. 7

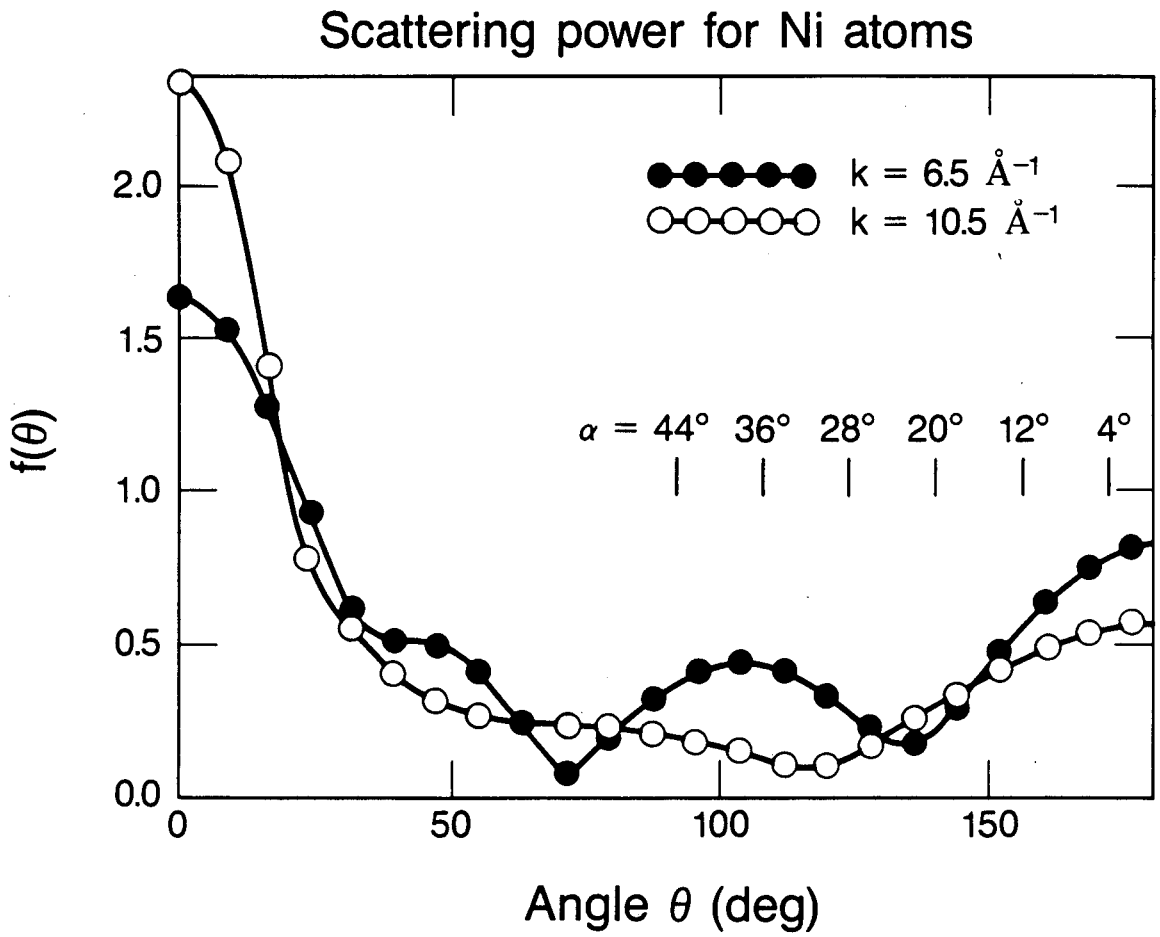

XBL 876-6336

Fig. 8

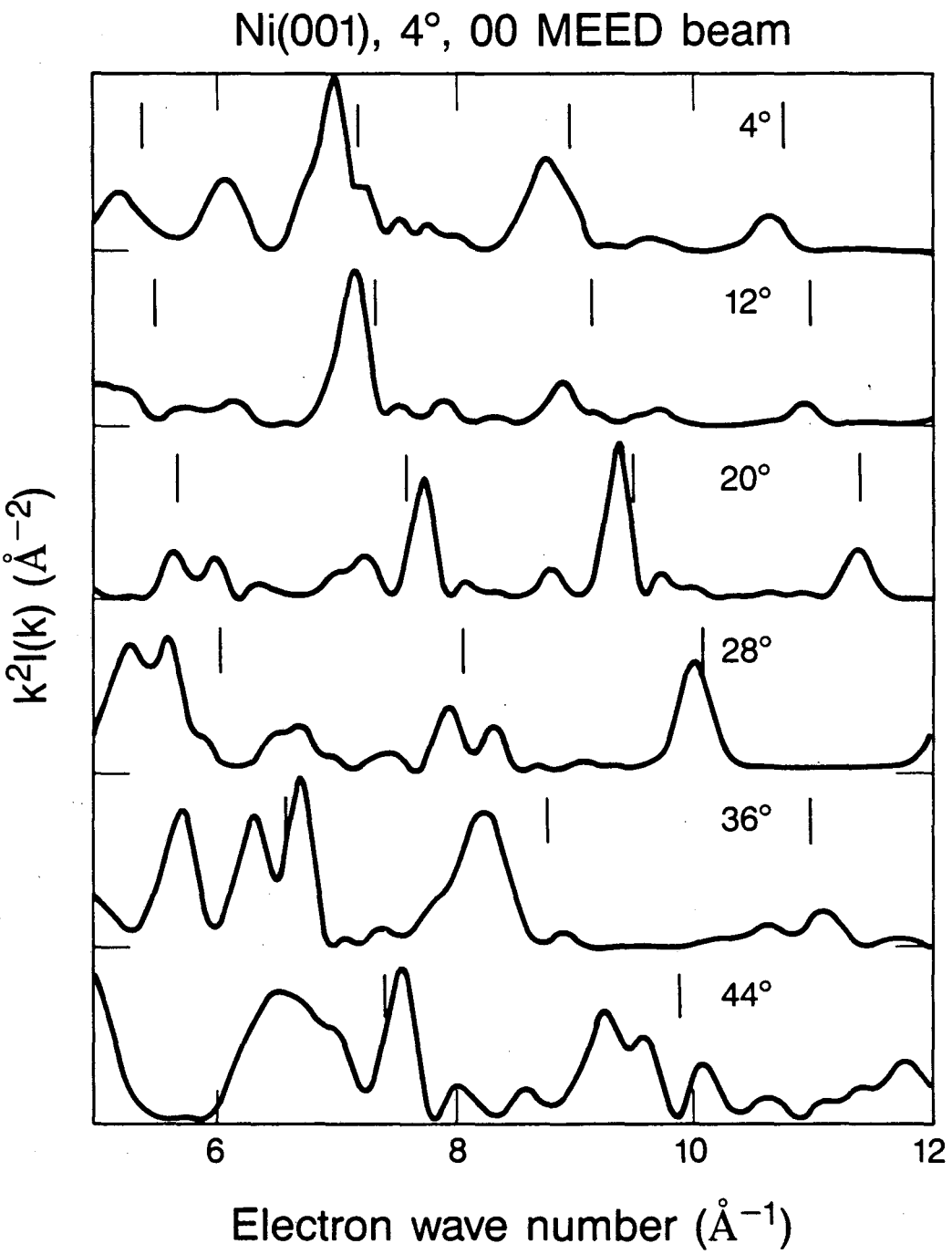

XBL 876-6340

Fig. 9

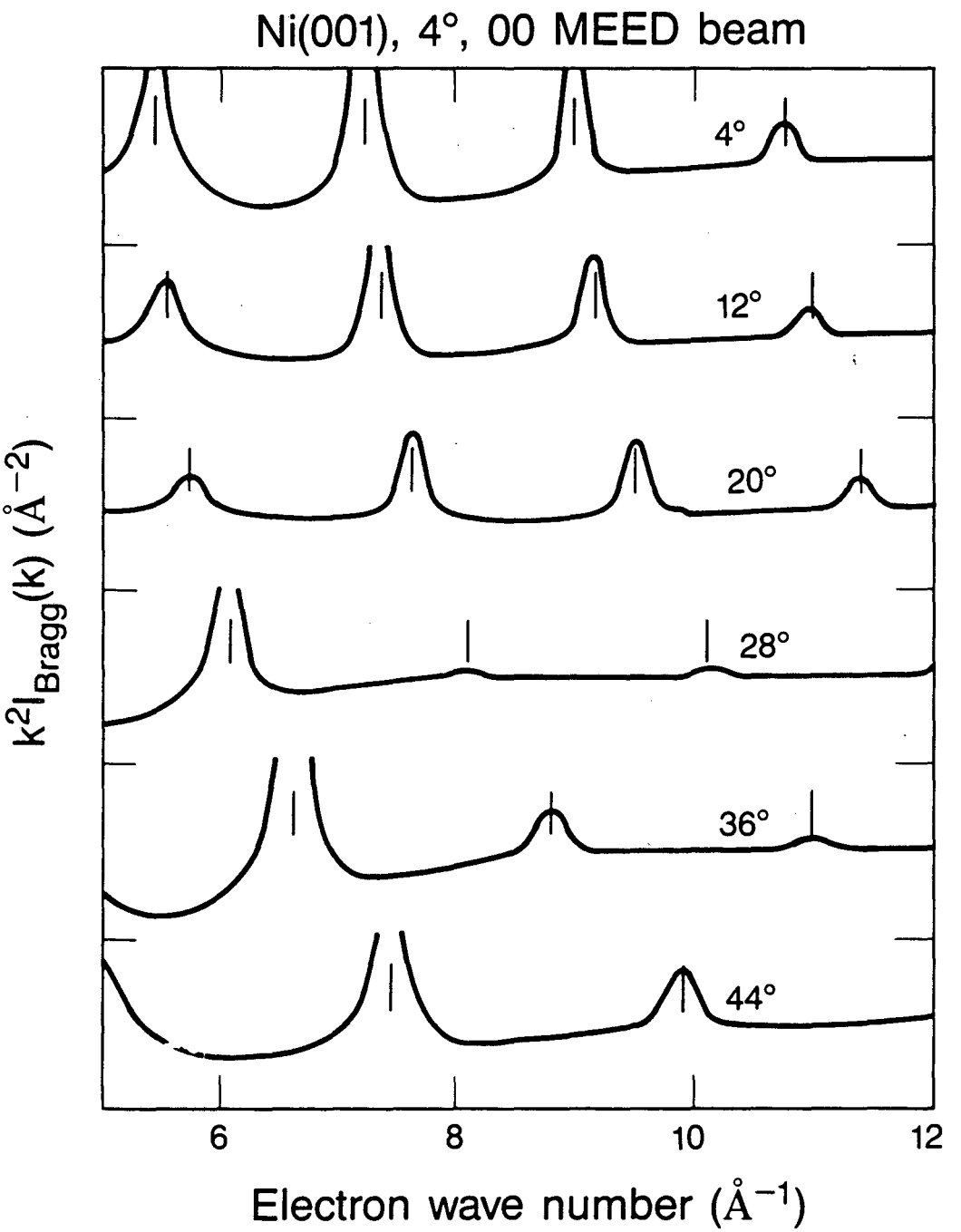

XBL 876-6337

Fig. 10

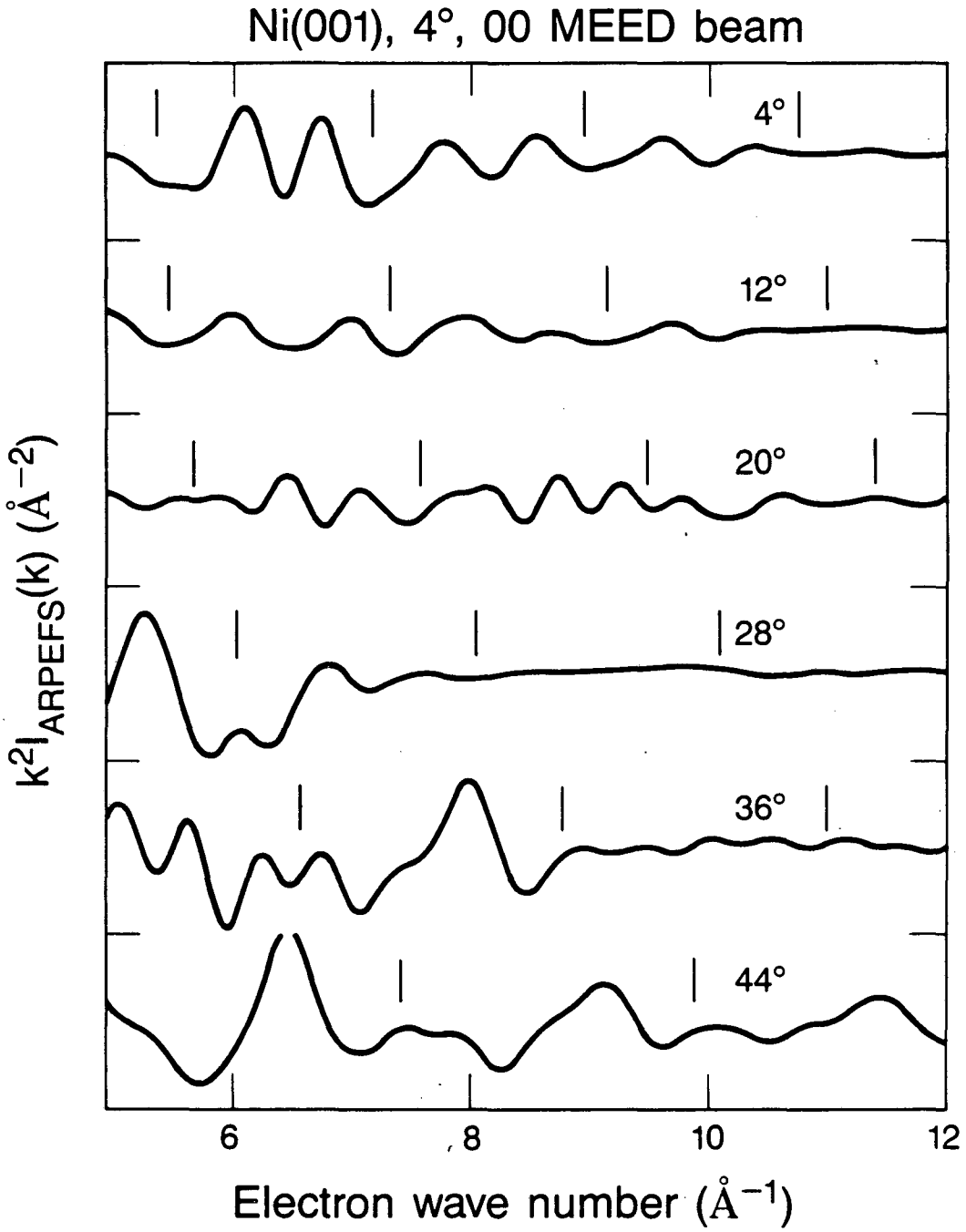

XBL 876-6338

Fig. 11

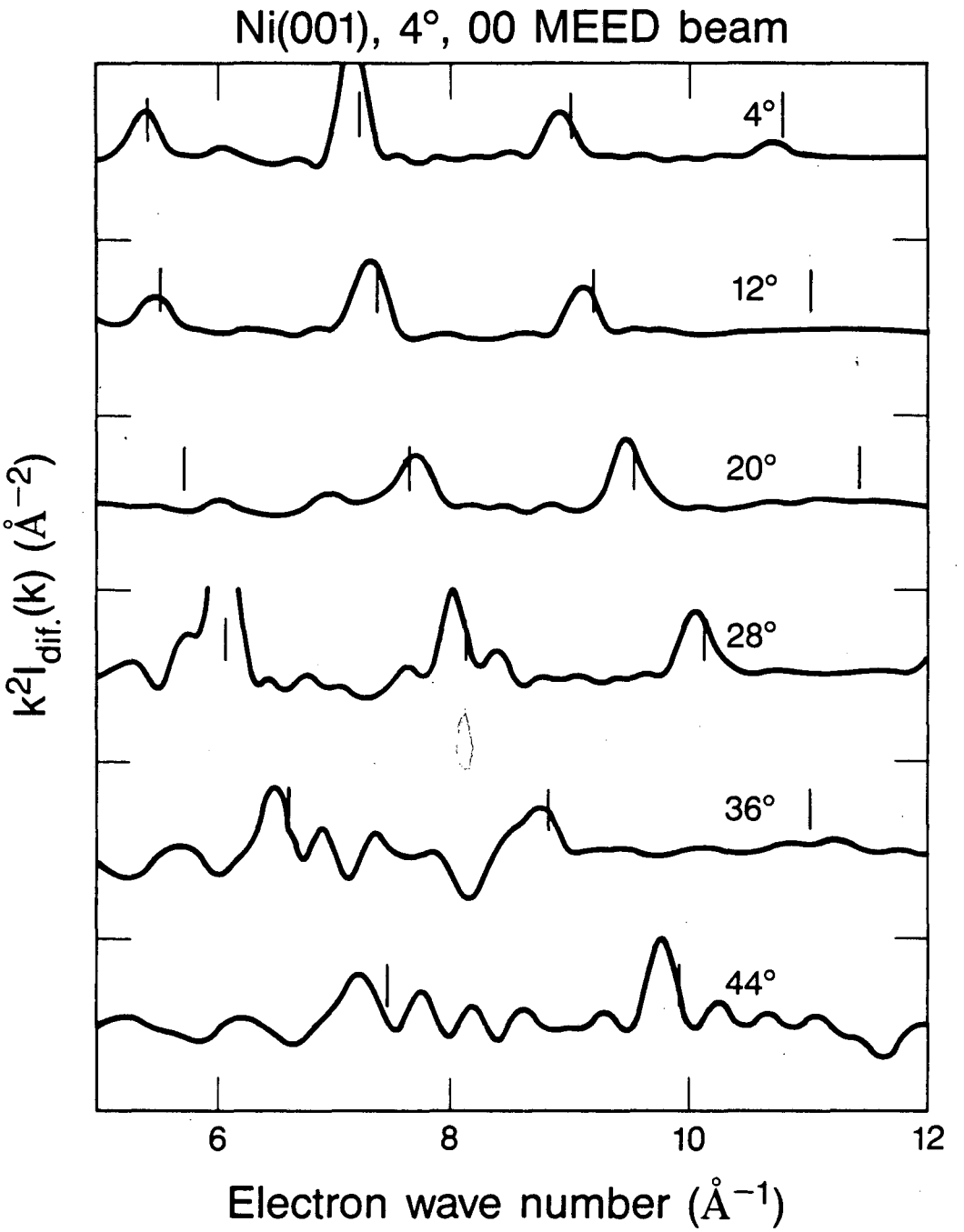

XBL 876-6339

Fig. 12

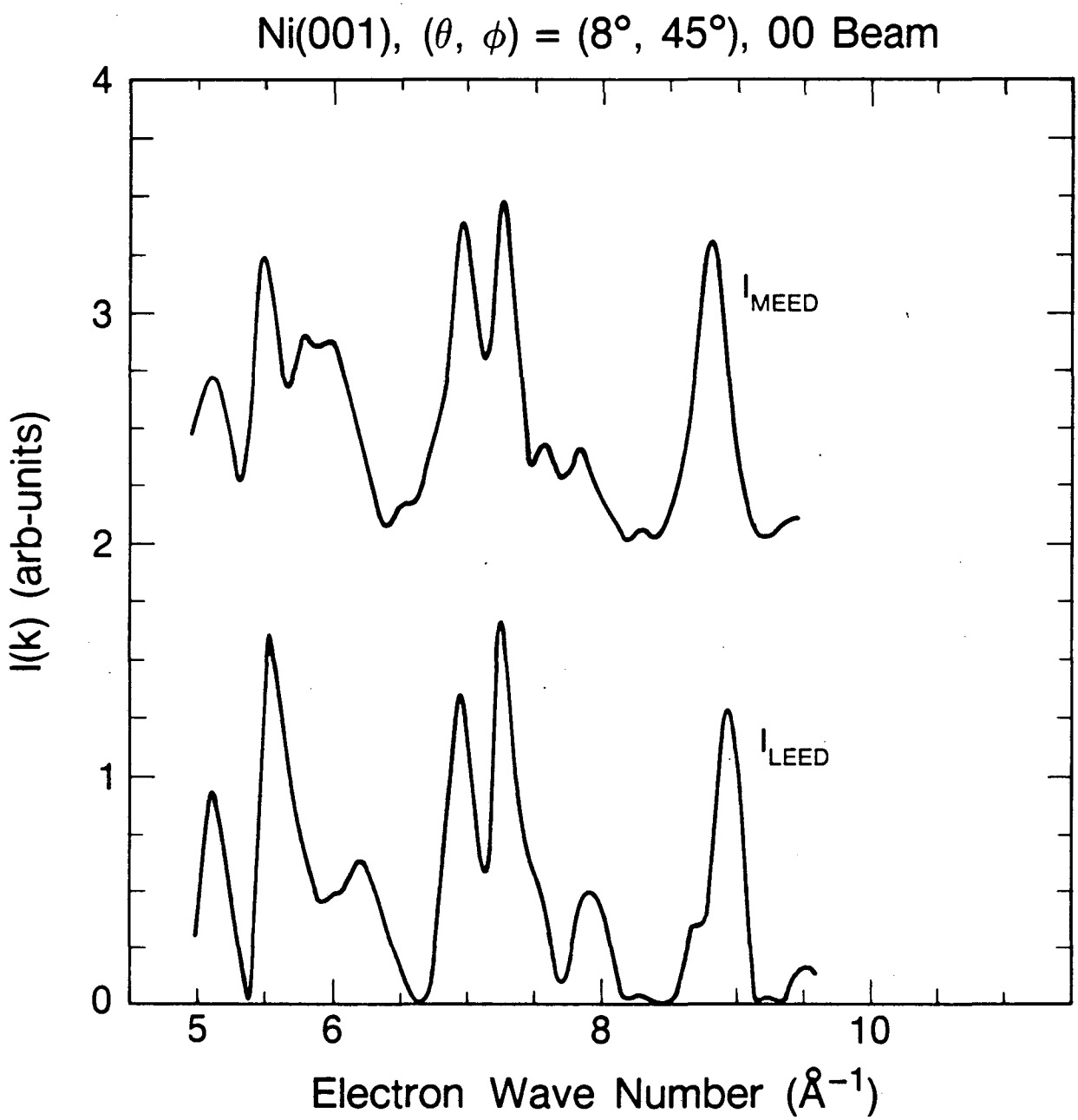

XBL 8712-9362

Fig. 13

LAWRENCE BERKELEY LABORATORY
TECHNICAL INFORMATION DEPARTMENT
UNIVERSITY OF CALIFORNIA
BERKELEY, CALIFORNIA 94720